The Atomic-scale Finite Element Method for Analyzing Mechanical Behavior of Carbon Nanotube and Quartz

Kyusang Kim

Thesis submitted to the faculty of the Virginia Polytechnic Institute and State University in partial fulfillment of the requirements for the degree of

Master of Science
In
Civil Engineering

Marte S. Gutierrez, Chair
Romesh C. Batra
Joseph E. Dove

August 22, 2006
Blacksburg, Virginia

Keywords: Atomic Scale, Finite Element Method, Molecular Dynamics, Mechanical Behavior, Carbon Nanotube, Quartz, Computational Mechanics, Atom

The Atomic-scale Finite Element Method for Analyzing Mechanical Behavior of Carbon Nanotube and Quartz

Kyusang Kim

ABSTRACT

The mechanical behavior of discrete atoms has been studied with molecular dynamics whose computational time is proportional to the square of the number of atoms, $O(N^2)$. Recently, a faster algorithm, Atomic-scale Finite Element Method (AFEM) with computational time proportional to the number of atoms, O(N), had been developed. The main idea of AFEM, compared with conventional finite element method is to replace nodes with atoms and elements with electric forces between atoms. When interpreting a non-linear system, it is necessary to use an iteration scheme.

A simulation of molecular dynamics based on the Verlet's method was conducted in order to validate AFEM in one dimension. The speed of AFEM was investigated in one and two dimensional atomic systems. The results showed that the computational time of AFEM is approximately proportional to the number of atoms, and the absolute computation time appears to be small. The frameworks of AFEM not only for multi-body potential but also pair potential are presented. Finally, AFEM was applied to analyze and interpret the mechanical behavior of a carbon nanotube and a quartz. The buckling behavior of carbon nanotube showed a good agreement with the results illustrated in the original literature.

Acknowledgement

During the first semester, I took the finite element course from my advisor, Dr. Marte S. Gutierrez. All the fundamental understanding about my research is from his teaching. I want to express my sincere gratitude for his belief in me. I also would like to thank my committee members, Dr. Romesh C. Batra and Dr. Joseph E. Dove for their kind responses to my questions. Dr. Jeff Wang is thanked for reviewing this thesis.

Dr. Hojong Baik, the research assistant professor in the air transportation system at Virginia Tech, encouraged me to use the vectorization scheme and sparse command. Mr. Hyun Shin explained the spring boundary condition. Mr. Matthew Sleep helped by reviewing this thesis. Dr. Hanqing Jiang, one of AFEM authors, answered my questions related to the energy minimization. I discussed about the potential energy functions with my fellow researcher, Mr. Alok Sharma. I deeply appreciate all of their help.

During my research, I shared my concerns with my Korean friends: Imsoo Lee, Soonkie Nam, Youngjin Park, Juneseok Lee, Youngki Kwon and Minchul Park.

This thesis is dedicated to my family: Byeongnam Kim, Hyosuk Heo, Kyuho Kim and Sunyoung Kim. I deeply thank Haejin Kim, my grandfather in heaven who was a friend and teacher of my life.

Table of contents

List of figures

List of tables

Chapter 1 Introduction

1.1 Background

"Nothing exists except atoms and empty space."

(Democritus, BC 460~ BC 370)

From ancient times, the fundamental source of materials was a question to philosophers and scientists. The atom they named meant the smallest particle which can not be divided. Now physicists and chemists have discovered that protons and neutrons are composed of quarks and even believe that quarks can be further divided into smaller elements.

It is surprising to imagine that all the materials in the world visible or invisible are made up of atoms. Even the human body is a combination of 65% oxygen, 18.5% carbon, 9.5% hydrogen and 3.2% nitrogen. It is obvious that the analysis at a smaller length scale will provide deeper insight into the behavior of materials. Enough experience of observing the forest has been accumulated, and it is time to see individual trees.

Recently, the study on materials at a small scale has been intensified by the development of the measurement science and information technology. As a measurement science, the scanning tunneling microscopy (STM) developed in 1981 brought us the opportunity to see the arrangement of atoms. Furthermore, desktop computers become faster and cheaper so that many researchers can simulate the behavior of atoms without much help of a supercomputer (Gates et al. 2005).

1.2 Geotechnical Issues in Nano-scale

In geotechnical engineering, the micro-scale behavior of soil has been investigated for its potential applicability to the stability of earth structures. There are biological effects, metal transport, creep in soil and some of the unusual phenomena such as quick clays, clay swelling, collapsing soils and thixotropy. These soil behaviors need further research combined with nano technology.

Microorganisms within soil can replicate themselves, depending on the amount of water and mineral, pH and temperature. The effects of microorganisms might increase the soil strength and decrease the hydraulic conductivity. Those positive mechanisms can be used to improve when geotechnical engineering is associated with the geochemistry and microbiology. For instance, the biologic force microscopy can be utilized for estimating the force between bacteria and mineral surfaces when observing the variation of bacteria with time. The state of ground previously analyzed with the three phases of solid, water, and air will be more clarified with biological consideration (Mitchell et al. 2005).

Containment transport has been an important issue as the environment suffers from waste disposal, acid mine drainage and industrial pollution. It has been reported that metals adhere to the surfaces of nano-particles when transported by advection and diffusion. Thus, depending on the size of nano-particles, the metals can be transported further than expected. (Hochella, 2001)

Kansai international airport in Japan completed in 1990 has experienced full secondary consolidation. Hydraulic jacks were prepared to support columns of the airport in order to prevent differential settlement. Recently, the x-ray diffraction analysis conducted by Ichikawa et al. (2004) disclosed that the main reason of the secondary settlement was the drainage of the interlayer water while the previous explanation was the breakage of the soil

skeleton. Furthermore, Ichikawa et al. verified the mechanism of their experiment with molecular dynamics simulation.

Some of the difficult questions existing in geotechnical engineering might be answered with nano-technology which includes four factors: the lattice structures, the electric forces between atoms, the chemical reactions and the biological effects. To improve our understanding of these four factors, the model based on the theory of physics, chemistry and biology should be compared with the experimental data. The mechanism of material behavior will be revealed with the continuous procedures of experiment, modeling and comparison between these two procedures (Gates et al. 2005).

1.3. Objectives of the Research

This research concentrates on the computational mechanics of materials which provides three advantages. First, if the mechanism of a material is known, its behavior under a certain circumstance can be predicted with a mathematical model. As a result, it will significantly reduce the number of laboratory tests, which usually requires a process of trial and error. The second benefit of the computational material science is that the properties of a new material can be predicted using the potential energy function and its parameters which can be used for the same atoms in other material. Finally, our understanding about a new material will be increased. Therefore, it is possible to avoid a conservative design due to our poor understanding about the characteristic of the material behavior (Gates et al. 2005).

The main objective of this research is the introduction and application of the atomic scale finite element method (AFEM) developed by Liu et al. (2003) to geotechnical engineering problems. AFEM is faster than other previous methods such as conjugate gradient method and molecular dynamics (MD). There are five objectives in this research.

• Validation of AFEM by comparing the stress-strain behavior with MD simulation in one dimension
• Study of the speed of AFEM in one and two dimensions
• Development of AFEM frameworks from one dimension to three dimensions
• Simulation of mechanical behavior of carbon nanotube
• Simulation of mechanical behavior of quartz

Chapter 2 Potential Energy Functions

2.1 Introduction

Force field methods, also named molecular mechanics simulate the movement of particles in a force field. Although it is reasonable to consider the forces exerted by electrons within atoms, the force field method ignores the behavior of electrons for the computational efficiency. To design the force field in nano-scale, we need to consider four basic factors controlling the energy between particles: Bond length, bond angle, rotation of bonds and non-bonded interaction as described in Figure 2.1. All of them depend on the relative motion of individual particles. The mathematical description of these potential energies is,

$$\phi(l,\theta,\omega,r) = \begin{cases} \sum_{bonds} \frac{k_1}{2}(L - L_0)^2 \\ + \sum_{angles} \frac{k_2}{2}(\theta - \theta_0)^2 \\ + \sum_{N} C_n(\cos(\ w)^n) \\ + \sum_{i=1}^{N} \sum_{j=i+1}^{N} \left(4\varepsilon_{ij} \left[\left(\frac{\sigma_{ij}}{r_{ij}} \right)^{12} - \left(\frac{\sigma_{ij}}{r_{ij}} \right)^{6} \right] + \frac{q_i q_j}{4\pi \cdot \varepsilon \cdot r_{ij}} \right) \end{cases} \tag{2.1}$$

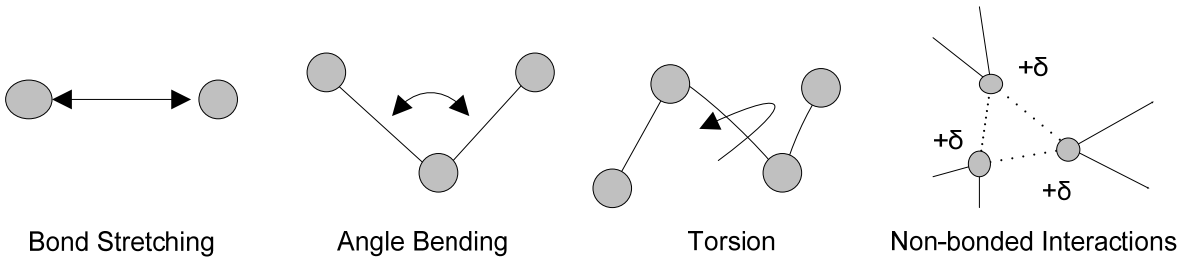

Figure 2.1 - Fundamental Mechanism of Designing Force Field

Equation 2.1 is the functional form standing for the bond stretching, angle bending, torsional term and electro-static interaction, respectively. L_0 is the reference bond length or natural length which makes bond stretching term zero. A related but different terminology is equilibrium bond length which refers to the state of minimum energy which can be obtained by minimizing the whole functional form between one atom and its neighboring atoms.

The potential energy function quantities such as k, n, ε, L_0, θ_0 and q are determined by studying atoms-atoms interaction. Determining these parameters is difficult due to the reproduction and transferability of lattice structures. The reproduction of lattice structures means that the lattice structure measured by X-ray diffraction should be regenerated with the force field and represented using suitable functional forms and corresponding parameters.

In this regard, those parameters and the functional forms can be applied to other different lattices if they have the same bonding. This is called transferability. For example, the Tersoff-Brenner potential is designed for the covalent bonding but the same functional form can be applied for hydrocarbon lattices, graphite, silica groups and diamond lattices although parameters used for each lattice are different (Tersoff, 1987). For the purpose of reproducing structural properties and transferability, the parameters and the functional forms are determined in an empirical way, with trial and error of computation.

The functional form has been developed, to account for both accuracy and efficiency of molecular simulation in a force field. An accurate simulation may require a huge computational time. For example, the electrostatic interaction influences atoms that are distant from one another, and it takes a long time to compute all the forces produced by surrounding atoms. Thus, there should be a balance between accuracy and efficiency (Leach, 2001).

2.2 Bond Stretching

2.2.1 Hooke's Law

One of the simplest potentials in bond stretching is Hooke's law model. Hooke's law states that the deformation of a material is linearly proportional to the external force. The potential energy and the internal force described by Hooke's law can be expressed by Equations 2.2 and 2.3, respectively.

$$\phi(x) = \frac{k}{2}(r - r_{eq})^2 + \phi_{\min} \tag{2.2}$$

$$f(x) = -\frac{d\phi}{dr} = -k(r - r_{eq}) \tag{2.3}$$

where ϕ and r represent the potential energy and the distance between particles, respectively, r_{eq} is the equilibrium distance between particles, and $\phi_{\min}$ stands for the minimum energy remained when each particle is in its the equilibrium position. The minimum energy is usually less than zero. The unit of energy equals the force times distance. Thus, the force can be derived from the first order derivative of energy with respect to distance.

In order to clarify the meaning of the energy and the force in Hooke's law model, the stiffness k=2, r_{eq} =1 and $\phi_{\min}$ =-1 were substituted into Equations 2.2 and 2.3, which are illustrated in Figures 2.2 and 2.3. In Figure 2.3, when the distance between particles is less than the equilibrium distance, the value of force is positive indicating it is a repulsive force because the positive internal force makes the particle move into the right direction in a conventional coordinate system. Outside the equilibrium distance, the internal force between particles becomes an attractive force. Wherever the particle is placed, the internal

force tends to move the particle towards the equilibrium position where the minimum energy exists unless external forces are applied.

The next example will help us understand the principle of the Atomic Scale Finite Element Method based on Newton's third law. Let us imagine that there is a ball on the graph of Figure 2.2 which looks like a receptacle. Regardless of the initial position of the ball, it will finally stop at the equilibrium point of the distance 1 after moving like a pendulum. If there is an external force acting in the left direction, the distance between the pair particles will be closer until the internal force equals the external force. On the contrary, if the external force makes the distance between particles greater than the equilibrium distance, the internal force will increase until it becomes the same as the external force. In short, no matter what an external force is, the ball will move toward a point where the net force becomes zero since the Newton's third law indicates that the sum of the external force and internal force is zero.

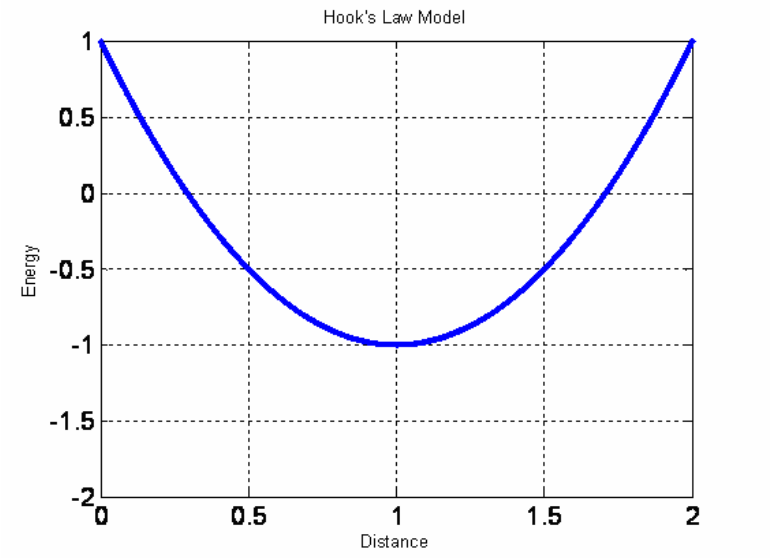

Figure 2.2 - Potential Energy between Particles in Hooke's Law Model

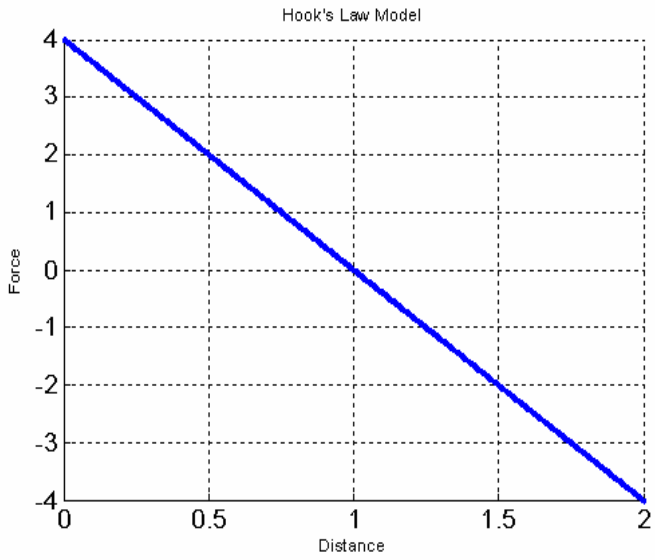

Figure 2.3 - Internal Force between particles in Hooke's Law Model

Hooke's law will be useful in a special case where displacement is small. The ultimate stress causes a fracture, making the material useless. This phenomenon cannot be explained by the Hooke's model since the attractive force increases as the distance between particles increases. In order to solve this problem, Lennard-Jones potential and Morse potential have been suggested.

2.2.2 Lennard-Jones Model

The Lennard-Jones model is used for calculating the interaction between two uncharged particles such as inert gases. The energy and force in Lennard-Jones model, respectively, are given by,

$$\phi(r_{ij}) = 4\varepsilon\left(\left(\frac{\sigma}{r_{ij}}\right)^{12} - \left(\frac{\sigma}{r_{ij}}\right)^{6}\right) \tag{2.4}$$

$$f(r_{ij}) = -\frac{\partial \phi}{\partial r_{ij}} = 4\varepsilon\left(12\left(\frac{\sigma^{12}}{r_{ij}^{13}}\right) - 6\left(\frac{\sigma^{6}}{r_{ij}^{7}}\right)\right) \tag{2.5}$$

where σ and ε stand for the equilibrium distance between particles and minimum energy, respectively. The minimum energy is required to separate two particles. With $f(r_{ij})=0$ in Equation 2.5, we can derive the equilibrium distance where no internal force exists. The equilibrium distance between particles calculated by Lennard-Jones potential is $\sqrt[6]{2}\sigma$.

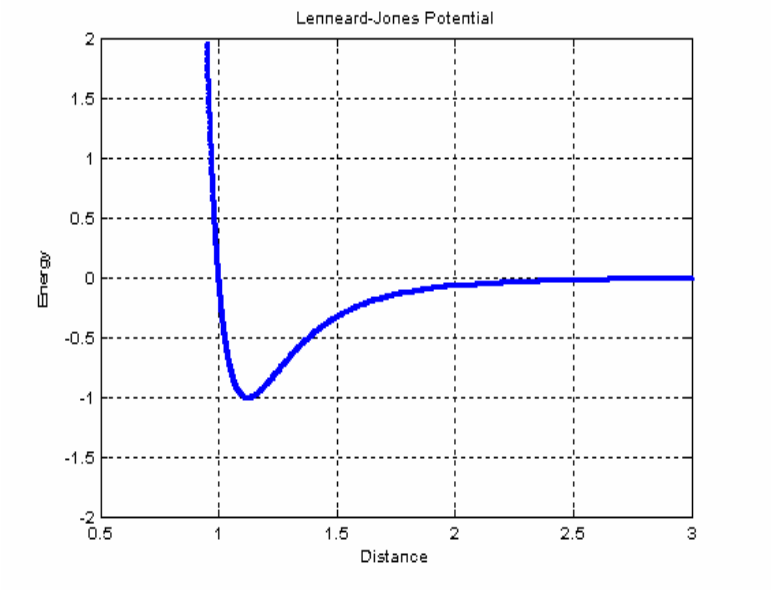

Figure 2.4 - Potential Energy between Particles in Lennard-Jones Model

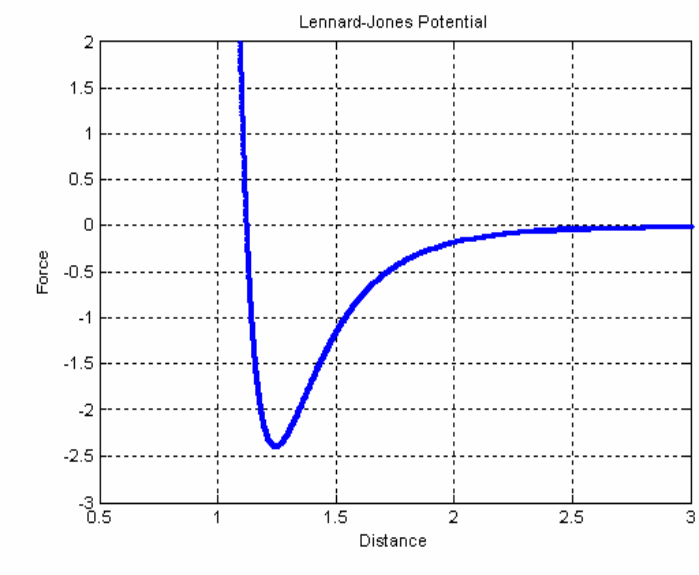

Figure 2.5 - Internal Force between Particles in Lennard-Jones Model

The $1/r^{12}$ term represents a strong repulsion based on the Pauli principle. The Pauli principle suggests that the electron clouds of atoms are difficult to be overlapped. If they share the orbital boundaries, there is a strong repulsion and a high energy between them. Thus, in order to minimize the high energy, particles tend to move away from each other. (Robinett, 1997)

The $1/ r^6$ term is based on van der Waals force which gives a weak attraction between atoms with a large distance between them. To simplify the Lennard-Jones model, $\sigma=1$ and $\varepsilon=1$ are generally substituted. From $f(r_{ij})=0$, the equilibrium distance is $\sqrt[6]{2}$, which is approximately 1.1225.

The Lennard-Jones potential shown in Figure 2.4 resembles a well. The depth of the well representing disassociation energy is defined as a distance between the minimal energy and zero energy. For example, the depth of the well is equal to 1 in Figure 2.4. Lennard-Jones

potential can be used to test algorithms since it shows a representative relationship between repulsive and attractive forces.

2.2.3 Morse Potential

While the Hooke's law provides the harmonic potential shown in Figure 2.2, Morse potential accounts for the bond breaking with the dissociation energy. It can be expressed as,

$$\phi(l) = D_e \{1 - \exp[-\alpha(L - L_0)]\}^2 \qquad (2.6)$$

where D_e is the depth of the potential energy minimum and α is $\omega(\mu/2\ D_e)^{0.5}$. ω and μ stand for the frequency of vibration and the reduced mass, respectively. If D_e, α, and L_0 take the value one in Equation 2.6, Figure 2.6 can be drawn, showing the variation of ϕ with L (Leach, 2001).

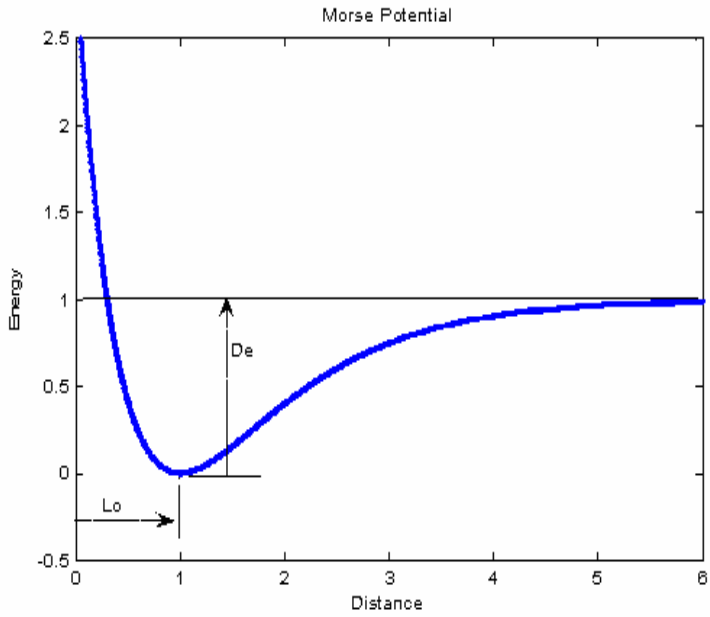

Figure 2.6 - Morse Potential Energy between Particles

2.2.4 Modified Born-Mayer-Huggins Potential

Silicon (Si) is the most abundant element followed by oxygen (O). These elements occupy more than 95 % of the earth crust. The oxygen atom has the strongest bond with the silicon atom. Si-O bond is the bonding between silicon and oxygen atom with a half being ionic bonding and the other half being covalent bonding. They are the fundamental sources of quartz, feldspars, amphiboles and micas. The most abundant mineral is quartz composed of silicon and oxygen atoms.

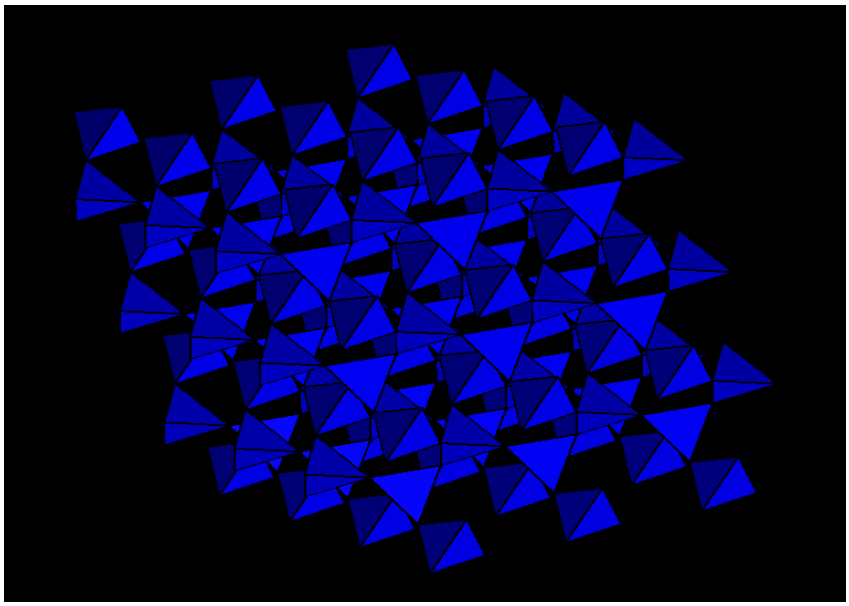

Figure 2.7 - Tetrahedrons of Quartz

Figure 2.7 shows the quartz structure, a group of tetrahedrons. The quartz structure changes, depending on the pressure and temperature. For instance, the low quartz exists under the temperature of 573 Celsius.

The modified Born-Mayer-Huggins (BMH) ionic potential has been suggested for analyzing the silica group. This is based on the Coulomb potential energy modified by the Ewald method. The two body potential function is,

$$\phi_{ij}(r_{ij}) = \sum_{i<j} (\frac{Z_i Z_j e^2}{r_{ij}}) erfc(\frac{r_{ij}}{\beta_{ij}}) + A_{ij} \exp(-\frac{r_{ij}}{\rho_{ij}}) \tag{2.7}$$

erfc is the complementary error function whose definition is given by,

$$erfc(x) = \frac{2}{\sqrt{\pi}} \int_x^\infty \exp(-t^2) dt \tag{2.8}$$

The parameters for Equation 2.7 are provided in Table 2.1.

Table 2.1 - Parameters for Modified Born-Mayer-Huggins Potential

	Si	O	Si-Si	Si-O	O-O
Z_i	4	-2	-	-	-
ρ_{ij} (nm)	-	-	0.029	0.029	0.029
A_{ij} (J)	-	-	1.877×10^{-16}	2.962×10^{-16}	0.7254×10^{-16}
β_{ij} (nm)	-	-	0.25	0.25	0.25

To improve our understanding of Equation 2.7, it is necessary to study the Ewald summation Method.

2.2.5 Ewald Summation Method

The long-range force represented by the Coulomb potential is believed to exist in ionic crystals like quartz. The charge-charge interaction included in the Coulomb potential can be expressed as,

$$\phi_{ij}(r_{ij}) = \frac{1}{2}\sum_{i=1}^{N}\sum_{j=1}^{N}\frac{q_i \cdot q_j}{4 \cdot \pi \cdot \varepsilon_0 \cdot r_{ij}} \tag{2.9}$$

where q_i and q_j are electric charges, r_{ij} is the minimal distance between two ions, and ε_0 is the electrical permittivity in space. Any ion interacts with all the other ions, which is accounted for in the Coulomb potential.

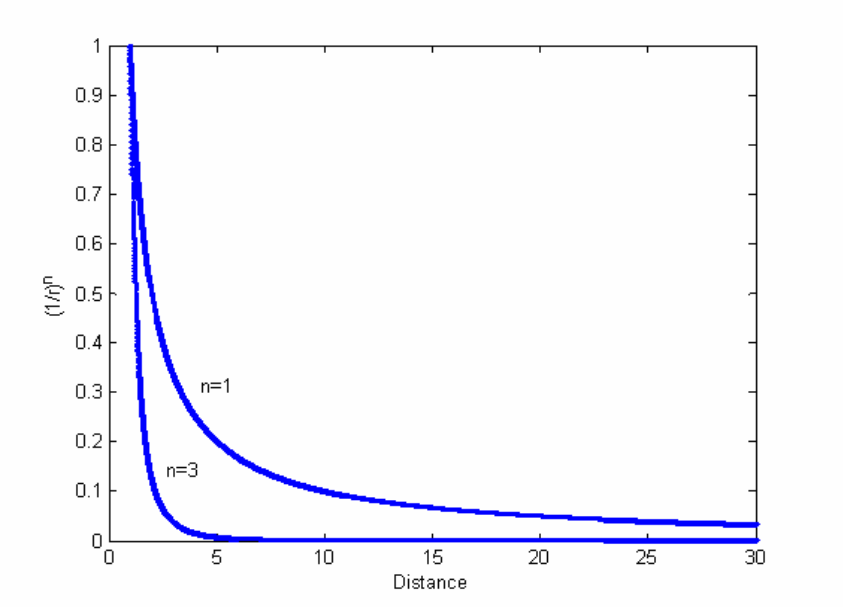

Figure 2.8 - Comparison between r^{-1} and r^{-3} with Distance

As an example, the variations of r^{-1} and r^{-3} against distance are compared in Figure 2.8. r^{-3} converges to zero at the distance of 5 while r^{-1} has a positive value even at the distance of 30. Since the Coulomb potential belongs to the case of r^{-1}, theoretically ions a long distance apart influence each other. Furthermore, the number of ions around one ion significantly increases if ions are continuously arranged in a three dimensional space. Therefore, the Coulomb potential requires enormous computational effort in order to estimate the potential energies of atoms.

A faster algorithm for this has been developed by Ewald (Leach, 2001). Ewald gave the formula expressed as,

$$\frac{1}{r} = \frac{f(r)}{r} + \frac{1-f(r)}{r} \tag{2.10}$$

With an appropriate function f(r), the first term in Equation 2.10 can be calculated in the real space, and the second term can be estimated in the reciprocal space. The Gaussian charge distribution used for f(r) is given by,

$$\rho_i(r) = \frac{q_i \alpha^3}{\pi^{3/2}} \exp\left(-\alpha^2 \cdot r^2\right) \tag{2.11}$$

Equation 2.11 neutralizes point charges considered by the Coulomb potential. The mathematical expression equivalent to Equation 2.9 can be written as,

$$\phi_{ij}(r_{ij}) = \begin{cases} \sum_{|n|=0}^{\infty} \frac{q_i \cdot q_j}{4 \cdot \pi \cdot \varepsilon_0} \frac{erfc(\alpha |r_{ij}+n|)}{|r_{ij}+n|} \\ + \sum_{|n|=0}^{\infty} \frac{q_i \cdot q_j}{4 \cdot \pi \cdot \varepsilon_0} \frac{4\pi^2}{k^2} \exp(\frac{k^2}{4\alpha^2}) \cos(k r_{ij}) \\ - \frac{\alpha}{\sqrt{\pi}} \sum_{k=1}^{N} \frac{q_k^2}{4 \cdot \pi \cdot \varepsilon_0} + \frac{2\pi}{3L^3} \left| \sum_{k=1}^{N} \frac{q_k^2}{4 \cdot \pi \cdot \varepsilon_0} \right|^2 \end{cases} \tag{2.12}$$

The first and second terms in Equation 2.12 represent the real space summation of f(r)/r and reciprocal summation of (1-f(r))/r in Equation 2.10, respectively. The third term in Equation 2.12 is to extract the Gaussian function which counts itself twice in the first term. The forth term reflects the medium outside of a simulation box. If there is a vacuum outside of the simulation box, it is required to consider the fourth term in Equation 2.12.

The first and second terms in Equation 2.12 are similar to Equation 2.7. Garofalini (1981) simplified Equation 2.12 and suggested Equation 2.7 which is called the screened Coulomb potential. The screened Coulomb potential significantly saves the computational time by assuming that the effect of an atom over a cutoff distance can be neglected. The cutoff distance of the modified Born-Mayer-Huggins potential is 5.5 Å.

2.3 Angle Bending

Following Hooke's law, angle bending due to change in orientation between atoms can be generated as:

$$\phi(\theta) = \frac{k}{2}(\theta - \theta_0)^2 \tag{2.13}$$

where k is a force constant and θ_0 is a reference angle. Compared with bond stretching, the angle bending requires less energy to cause deformation. Furthermore, as illustrated in Table 2.2, the force constant increases with an increasing bonding strength, and the reference angle varies in different structures due to different atomic bonds (Leach, 2001).

Table 2.2 - Constants of Angle Bending with Different Bonding (Allinger, 1977)

Angle	k (kcal mol^{-1} deg^{-1})	θ_0 (degree)
Csp^3-Csp^3-Csp^3	0.0099	109.47
Csp^3-Csp^3-H	0.0079	109.47
H-Csp^3-H	0.0070	109.47
Csp^3-Csp^2-Csp^3	0.0099	117.2
Csp^3-Csp^2=Csp^2	0.0121	121.4
Csp^3-Csp^2=O	0.0101	122.5

2.4 Torsional Terms

The torsional term is less widely used than the bond stretching and the angle bonding. The torsional term prevents the lattice structure from twisting. It considers the angle displacement between two elements like the angle bending, but the two elements are separated by a distance of another element. It might be possible to substitute the non-bonded interactions with the torsional terms, and it will significantly reduce the computational time. The basic equation of the torsional terms is,

$$\phi(\omega) = \sum_{n=0}^{N} \frac{V_n}{2}\left[1 + \cos(n\omega - \gamma)\right] \tag{2.14}$$

where $V_{n,}$ ω and γ are the barrier height, torsion angle and phase factor, respectively. The barrier height works to keep the torsion angle stay where the minimum energy exists. Thus, a high barrier height represents a strong resistance against a torsional force.

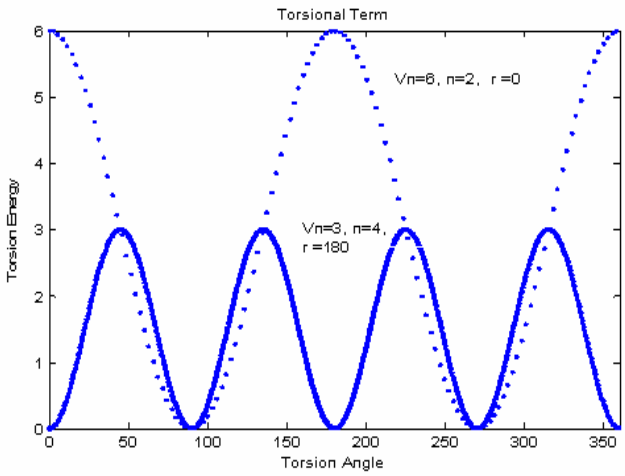

Figure 2.9 - Single Torsional Potential with Different Values of $V_{n,}$ ω and γ

Figure 2.9 shows that the single torsional terms vary with $V_{n,}$ ω and γ. The parameter n implies how many times the minimum energy occurs as the torsion angle changes. For example, minimum energy occurs twice in the case of dotted line at angles of 90° and 270 ° while minimum energy occurs four times in the case of solid line at angles of 0°, 90°, 180° and 270°. As a result, these constants are used to determine how much torsional angles should be changed to stabilize specific lattice structures.

2.5 Cross Terms

The cross terms are composed of stretch, bend and torsion functions. The main idea is that the energy exerted in one element between two atoms is associated with the movement of other neighboring atoms. This is also the major concept of the multi-body potential. Usually the two terms are expressed as two multiplied terms. Since the change of energy in one term significantly influences the other, the cross term represents a stronger bonding suitable for the covalent bonding. It has been reported that stretch-stretch, stretch-bend and stretch-torsion terms are commonly used in molecular dynamics. The bend-bend-torsion term is rarely used. The stretch-stretch term can be described as,

$$\phi(l_1, l_2) = \frac{k}{2}(l_1 - l_0)(l_2 - l_0) \tag{2.15}$$

Likewise, the stretch-torsion cross term can be expressed as,

$$\phi(l, \theta) = k(l - l_0)(\cos n\omega) \tag{2.16}$$

The stretch-bending term crossing the length and angle term is,

$$\phi(l_1, l_2, \theta) = \frac{k}{2}\left[(l_1 - l_0) + (l_2 - l_0)\right](\theta - \theta_0) \tag{2.17}$$

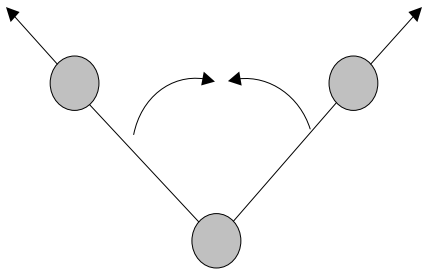

Figure 2.10 - Stretch-Bending Term

In Figure 2.10, the stretch-bending term is illustrated. It was developed as a substitute for the covalent bonding materials such as the carbon nanotube and the diamond. The Tersoff-Brenner potential is one of stretch-bending terms.

2.6 Tersoff-Brenner Potential

The pair potentials such as Lennard-Jones potential and exponential Morse potential were originally developed for simple metals, gases and ions. Thus, it does not reflect the characteristics of the covalent bonding. Tersoff (1987) suggested the potential energy function for the covalent systems which is observed in semiconductors, ceramic and polymers. Consequently, Brenner (1990) developed a potential to analyze the carbons and hydrocarbons. Brenner adopted the Tersoff's potential in order to reproduce the covalent systems such as diamond, graphite and hydrocarbons.

Brenner proposed three objectives in developing the potential function suitable for the covalent system. The potential should regenerate the energy and structure of diamond, graphite and hydrocarbons. It should also be necessary to exhibit the bond breakage and

forming. Moreover, the energy of one atom should depend on the first and second neighboring atoms in order to save the computational time. (Brenner, 1990)

The carbon nanotube (CNT) consists of carbons and has the graphite structure. Therefore, the Tersoff-Brenner potential and its parameters can be used to analyze the CNT. The multi-body interatomic potential including the bond angle has the following basic formula:

$$V(r_{ij}) = V_R(r_{ij}) - \overline{B}_{ij} V_A(r_{ij}) \tag{2.18}$$

where the subscripts R and A stand for the repulsive and attractive energies, respectively. It has a similar structure to Lennard-Jones potential. The difference lies in terms added to the bond stretching term. The Tersoff-Brenner potential is composed of the Morse term for stretching and angle bending while a higher order distance function is used in Lennard-Jones Potential. The repulsive and attractive terms in the Tersoff-Brenner potential are provided by,

$$V_R(r_{ij}) = \frac{D^{(e)}}{S-1} \exp\left[-\sqrt{2S}\beta(r-R)\right] f_c(r) \tag{2.19}$$

$$V_A(r_{ij}) = \frac{D^{(e)} S}{S-1} \exp\left[-\sqrt{\frac{2}{S}}\beta(r-R)\right] f_c(r) \tag{2.20}$$

B_{ij} is the multi-body coupling function involving angle terms and is given by,

$$B_{ij} = \left[1 + \sum_{k(\neq i,j)} G(\theta_{ijk}) f_c(r_{ik})\right]^{-\delta} \tag{2.21}$$

k is a node number of an atom adjacent to atoms i and j as illustrated in Figure 2.11. r_{ik} is the distance between atoms i and k. The function G containing the angle bending terms is given by,

$$G(\theta_{ijk}) = a_0\left[1+\frac{c_0^2}{d_0^2}-\frac{c_0^2}{d_0^2+(1+\cos\theta_{ijk})^2}\right] \tag{2.22}$$

θ_{ijk} represents the angle between elements ij and ik. Finally, in order to save the computational time, a smooth cut-off function, $f_c(r)$, was employed and expressed as,

$$f_c(r) = \begin{cases} 1 & r < R^{(1)} \\ \frac{1}{2}\left\{1+\cos\left[\frac{\pi(r-R^{(1)})}{R^{(2)}-R^{(1)}}\right]\right\} & R^{(1)} < r < R^{(2)} \\ 0 & r > R^{(2)} \end{cases} \tag{2.23}$$

The smooth cutoff starts from $R^{(1)}$=0.17 nm and ends at $R^{(2)}$=0.2 nm. The atoms i and j have different local environments, and it is necessary to devise the symmetric function by averaging B_{ij} and B_{ji},

$$\overline{B}_{ij} = \frac{(B_{ij}+B_{ji})}{2} \tag{2.24}$$

To improve our understanding about B_{ij} and G factors, it is necessary to illustrate the lattice structure of the CNT, as shown in Figure 2.11.

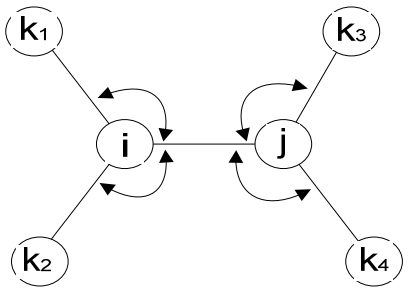

Figure 2.11 - Part of Carbon Nanotube Structure with Angle Bending

The bond strength depends on the local environment of the system. For example, in Figure 2.11, the energy stored between atoms i and j is affected by other atoms such as k_1, k_2, k_3 and k_4 surrounding the atoms i and j by the angle bending. In other words, the atom i has a different potential energy as the locations of atoms k_3 and k_4 change. Likewise, the potential energy of the atom j depends on not only atom i but also on atoms k_1 and k_2. This multi-body potential provides the mechanism to stabilize the structure through the angle bending. The parameters used in the Tersoff-Brenner potential for the CNT are listed in Table 2.3 (Brenner, 1990).

Table 2.3 - Parameters of Tersoff-Brenner potential for CNT

$R^{(1)}$	0.17 nm	S	1.22
$R^{(2)}$	0.2 nm	β	21 nm^{-1}
$D^{(e)}$	6 eV	a_0	0.00020813
$R^{(e)}$	0.1390 nm	c_0	330
δ	0.5	d_0	3.5

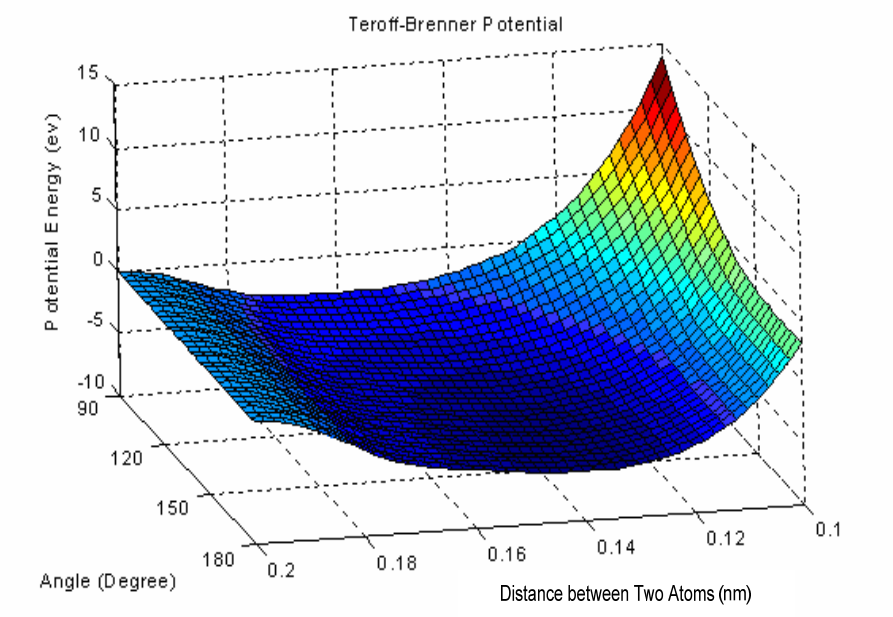

Figure 2.12 - Tersoff-Brenner Potential with Various Distances and Angles

The Tersoff-Brenner potential was described using various distances and angles in Figure 2.12. The potential energy was designed to increase with an increasing angle between elements and to achieve the lowest value at a distance of 0.14 nm. It turns out that as the angle increases, the corresponding atomic distance at the lowest energy also changes on the surface of the energy plane shown in Figure 2.12. It is important to note that the potential energy does not necessarily indicate the lowest energy point. The critical location is a point where the tangent to the energy surface has zero slope. In fact, in most cases, due to the hexagonal shape of the CNT structure, each angle approximately ends at 120 degrees.

Chapter 3 Literature Review

3.1 Introduction

Molecular Dynamics (MD) has provided a deeper understanding of materials at the atomic level since the 1950s. The starting point of analyzing the motion of molecules began with the invention of computers. The development of numerical analysis and the improvement of the capacity of computers made it possible to simulate the chemical reactions, droplet formation, fluid flow and phase transitions.

In the late 1950s, for the first time the hard spear model was created by Alder and Wainwright at Lawrence Livermore National Laboratory (Alder, 1959). This method regards the molecules as balls. Similar to billiard balls which collide on the table, the molecules move along straight lines and collide with each other. While they change their velocities and directions after collision, the total momentum and total energy should be conserved. Because after every collision of one molecule, the distance between entire particles should be calculated again, the hard spear method consumes too much time and memory of computer.

Thermodynamics and physical chemistry started to employ Molecular Dynamics (MD) to examine the collective behavior of solids, gases and liquid. MD was born with the assumption that the atomic interaction depends on the orientation and distance between atoms, and the total mass in a system is constant. The Euler and Verlet method are traditionally used for numerically integrating the acceleration with respect to time.

Recently, a faster algorithm called atomic-scale finite element method has been developed, united with the finite element method and iterative methods. Although this method does not contain a time-dependent behavior of MD, it can calculate the mechanical behavior of crystal line structures faster than other methods.

3.2 Molecular Dynamics

3.2.1 Euler's Method

Molecular Dynamics method is based on the Newton's second law which can be expressed as,

$$f(x) = m \cdot \ddot{x} \tag{3.1}$$

The function f(x), m and x indicate the force, mass and distance, respectively. In addition, the first and second derivatives of distance in terms of time represent the velocity and acceleration, which are $\dot{x}$ and $\ddot{x}$, respectively. Then we need two initial conditions,

$$x(0) = x^{(0)}, \dot{x}(0) = \dot{x}^{(0)} \tag{3.2}$$

From Taylor's expansion, the next position of particles can be evaluated with time interval of h, expressed as,

$$x(t+h) \approx x(t) + h\dot{x}(t) \tag{3.3}$$

$$\dot{x}(t+h) \approx \dot{x}(t) + \frac{h}{m} f\left(x((t))\right) \tag{3.4}$$

The force divided by mass provides the acceleration according to Newton's second law. Then integrating the acceleration by time once and twice gives velocity and distance, respectively. If the time interval of h approaches zero, the preceding equations will provide an exact solution. However, a small time step of h greater than zero is used and in turn, causes truncation and discretization error. Error directly depends on the size of h, and the error of Euler's method turns out to be O(h). This error is considered to be large, and it is

necessary to find out a more accurate computational method. The most commonly used method in Molecular Dynamic is Verlet's method (Fosdick, 1995).

3.2.2 Verlet's Method

Verlet's method is actually based on Störmer's method in Mathematics. The second derivative of distance with finite difference can be expressed as,

$$\ddot{x} = \frac{x(t+h) - 2 \cdot x(t) + x(t-h)}{h^2} \tag{3.5}$$

If this equation is rearranged in terms of x(t+h),

$$x(t+h) \approx 2 \cdot x(t) - x(t-h) + \frac{h^2}{m} \cdot f(x(t)) \tag{3.6}$$

In Euler's method, the velocity and the position of atoms are calculated separately, and the next position is determined by the present position and velocity. However, Verlet's method is performed by not only the present position but also the past location of particles in order to predict the next position more accurately. In addition, Taylor's series expansion to the first three terms is used:

$$x(t+h) \approx x(t) + h \cdot \dot{x}(t) + \frac{h^2}{2 \cdot m} f(x(t)) \tag{3.7}$$

If Equations 3.6 and 3.7 are combined, the next algorithms are derived for simulating the Molecular Dynamics.

$$x(t+h) \approx x(t) + h \cdot \left(\dot{x}(t) + h \cdot \frac{f(x(t))}{2 \cdot m} \right) \tag{3.8}$$

$$\dot{x}(t+h) \approx \dot{x}(t) + \frac{h}{2 \cdot m} \cdot \left\{ f(x(t+h)) + f(x(t)) \right\} \tag{3.9}$$

In order to launch this algorithm, the initial condition is needed, as Equation 3.2 in Euler's method. For energy iteration, we need to calculate Equations 3.8 and 3.9. Equation 3.8 provides the next position of atoms, and Equation 3.9 gives the velocity of atoms in the next step. Equation 3.9 is not used in the present step but is saved for substituting $\dot{x}(t)$ in Equation 3.8 in the next iteration. As a result, although it provides more accurate result, one more calculation per iteration is needed.

The first three terms in Taylor's expansion of Equation 2.26 are used for simulating the Molecular Dynamics system. Unlike Euler's method, which manipulates the first two terms, the error of Verlet's method depends on h^2 in the third term of Equation 3.7. Thus, the error of Verlet's method is $O(h^2)$.

3.3 The Atomic-scale Finite Element Method (AFEM)

3.3.1 Principle of AFEM

The atomic scale finite element method (AFEM) is based on the finite element method. It treats nodes as atoms and elements as electric forces between atoms. The particles move toward the place where there is a smaller energy, and the energy minimization at the final stage can be expressed as,

$$\frac{\partial E_{tot}}{\partial x} = 0 \tag{3.10}$$

The potential energy depends on the distance between atoms. The electric energy stored in the atomic bonds is,

$$U_{tot} = \sum_{i<j}^{N} U(x_j - x_i) \tag{3.11}$$

If there are externally applied forces, the total energy consists of the internal and external energy which can be written as,

$$E_{tot}(x) = U_{tot}(x) - \sum_{i=1}^{N} \bar{F}_i \cdot x_i \tag{3.12}$$

With an initial guess of the atomic position, ($x^{(0)} = (x_1^{(0)}, x_2^{(0)}, ..., x_N^{(0)})^T$), the Taylor's expansion to the first three terms approximately represents the equilibrium state as,

$$E_{tot}(x) = E_{tot}(x^{(0)}) + \left.\frac{\partial E_{tot}}{\partial x}\right|_{x=x^{(0)}} \cdot (x - x^{(0)}) + \frac{1}{2} \cdot (x - x^{(0)})^T \cdot \left.\frac{\partial^2 E_{tot}}{\partial x \partial x}\right|_{x=x^{(0)}} \cdot (x - x^{(0)}). \tag{3.13}$$

After the third term in the right side of Equation 3.13 is omitted, Equation 3.13 is substituted into Equation 3.10. Then with the displacement of $u=x-x^{(0)}$, the equation similar to the framework of the finite element method can be derived as,

$$K \cdot u = P \tag{3.14}$$

where

$$K = \left.\frac{\partial E_{tot}}{\partial x}\right|_{x=x^{(0)}} = \left.\frac{\partial^2 U}{\partial x \partial x}\right|_{x=x^{(0)}} \tag{3.15}$$

$$P = -\left.\frac{\partial E_{tot}}{\partial x}\right|_{x=x^{(0)}} = \overline{F} - \left.\frac{\partial U_{tot}}{\partial x}\right|_{x=x^{(0)}} \tag{3.16}$$

K is the stiffness matrix, and P is the non-equilibrium force vector. This concept is the same as the finite element method if the nodes are considered as atoms and elements as the force relationship between atoms exerted by potential energies. In case of a linear system, one iteration will give the equilibrium position of particles, but the non-linear systems need several iterations until P vector approaches zero, P=0. (Liu et al, 2003)

As seen in the previous explanation, the third terms and higher in Taylor expansion were eliminated for the application of the finite element method developed for interpreting the linear relationship between force and displacement, K·u=P. This approximation employs the iteration method in order to follow the non-linear relationship between force and displacement with the linear calculation of the finite element method. The main idea is that through the repetition, the distances between particles are optimized, and atoms approach to minimal energy points.

3.3.2 Computational Procedure of AFEM

In the simple equation of Ku=P, K and P should be expanded to matrix and vector forms, respectively, in order to transform many atoms from the non-equilibrium position to the equilibrium state. In one dimensional AFEM, for example, N atoms makes the global stiffness K matrix with a size at (N, N) and P vector with (N, 1).

The computation involved in AFEM is divided into 3 parts. The first step is to construct the K matrix and the P vector. In the next step, we solve the equation Ku=P. The displacement u is calculated by multiplying the inverse of K matrix by the non-equilibrium force vector, P. Finally, the displacement of $u=x-x_0$ is added to the original position of atoms. In this way, at every iteration, the atom moves until P=0. P vector consists of the external force of F and the internal force of $\partial U/\partial x$. Thus P=0 represents the equilibrium state when the external force and internal force are the same, satisfying the Newton's third law.

3.3.3 Computational Time of AFEM

AFEM follows three steps for computation and it is directly associated with the computational effort and time. The first computational time of AFEM is spent on constructing the stiffness matrix K and non-equilibrium vector P. If N is the number of atoms, the computational time for this is proportional to N. In addition, if the stiffness K matrix is sparse, solving Ku=P also takes time proportional to N. The number of steps to solve the problem with a computer program is called time complexity and in this case, the computational time proportional to N can be expressed by the notation of O(N) used in computer science. One more thing to consider for the computational speed is the iteration step.

The number of iterations significantly depends on the form at the interatomic potential. For example, in case of the linear system such as the interatomic potential based on Hook's law, only one iteration is needed to find the equilibrium state of atoms. Most of the interatomic potentials, however, show a non-linear relationship between the internal force and the locations between atoms in order to reflect the realistic nature of a material. To analyze the non-linear system with AFEM, it is necessary to perform M iterations until the P vector

converges to zero. Thus, the total computational speed of AFEM is O(M*N). It has been reported that the number of iterations M is independent to the number of particles. Regardless of the number of the atoms in a system, M is approximately constant. In case of the carbon nanotube, the iteration steps of M range from 31 to 43. Since M is constant and relatively small compared with the number of atoms, AFEM can be applied to the system involving a larger number of atoms (Liu et al. 2003).

There are several factors to be pointed out, affecting the iteration step although their effect might not be significant. They are basically due to different distances between the initial and the final position of particles. For instance, the initial position of atoms can influence the iteration step. If the distance between the initial state of particles and the position at equilibrium is longer, it requires more iterations. The slope of the energy surface also affects the number of iterations since the global stiffness matrix, K, which represents the gradient of the force vector, is different. Furthermore, the external force has a similar effect on M like the initial position of particles because it changes the P vector. For example, if the external force is applied to the atoms at equilibrium, a larger magnitude of the external force would cause a larger displacement of particles, and in turn, additional iterations (Liu et al. 2003).

3.3.4 Stability of AFEM

It is important to keep the AFEM system stable. The AFEM system is stable if the stiffness matrix is positively definite. However, due to the bifurcation effect or stress-strain softening, there might be a negative value in diagonal position of the stiffness matrix.

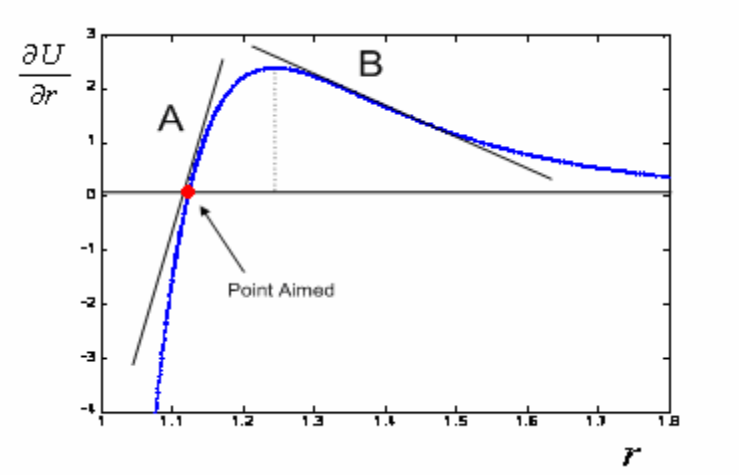

Figure 3.1 - Value of Stiffness Depending on Distance between Atoms

The stiffness K can be interpreted as the gradient $\partial U / \partial r$. The value of stiffness depends on the distance between atoms. For example, in Figure 3.1, the slope at A is positive, while the slope at B is negative. The negative slope at B is undesirable since it will make the distance between atoms further away than the point aimed in Figure 3.1. In that case, it is necessary to modify the stiffness matrix by substituting K with K+ α*I. I is the identity matrix, and α is a positive number large enough to make the stiffness matrix positive definite.

3.3.5 Multibody Interatomic Potential

Some of the potentials include the multibody interaction by considering the angle bonding. In order to implement the potential used in MD, it is important to devise the AFEM employing multibody interatomic potential. The interatomic potential acting on an atom is affected by the locations of atoms surrounding it. It can be described as,

$$U_{tot}(x) = \sum_{i<j}^{N} U(x_j - x_i; x_k - x_{i,} k \neq i, j) \tag{3.17}$$

where $x = [x_1, x_2, \ldots, x_N]$ stands for individual locations of all atoms. This formula expresses that the energy of an atom is associated with not only the distance between atoms i and j but also element between atoms i and k. The atom k is a second nearest atom or an atom located further than the second nearest neighboring atoms.

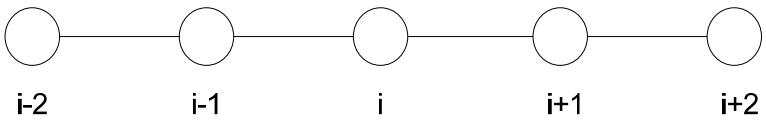

Figure 3.2 - One-dimensional Atomic Chain

For instance, the one-dimensional chain in Figure 3.2 was sketched, and the corresponding multi-body interatomic potential function is,

$$U_{(i-1,i)} = U\left(x_i - x_{i-1}; x_{i-1} - x_{i-2}\right) + U\left(x_i - x_{i-1}; x_{i+1} - x_i\right) \tag{3.18}$$

Equation 3.18 is a simple expression of Equation 3.17, considering the second nearest atoms. It represents that the energy stored in atom i is influenced by the nearest neighboring atoms such as atom i-1 and i+1 as well as the second nearest atoms such as atoms i-2 and i+2. Thus, the first derivative of the potential energy stored in i can be expressed as,

$$\frac{\partial U_{tot}}{\partial x_i} = \frac{\partial\left(U_{(i-2,i-1)} + U_{(i-1,i)} + U_{(i,i+1)} + U_{(i+1,i+2)}\right)}{\partial x_i} \tag{3.19}$$

3.3.6 Framework of One-dimensional AFEM for Multibody Potential

The total energy of atom i is the sum of all energies supplied by elements located between atoms from i-2 to i+2. This overlapping scheme provides a more stable atomic structure. The corresponding stiffness matrix and nonequilibrium force vector in one dimensional AFEM can be derived as:

$$\begin{bmatrix} \frac{\partial^2 U_{tot}}{\partial x_i \partial x_i} & \frac{1}{2}\frac{\partial^2 U_{tot}}{\partial x_i \partial x_{i-2}} & \frac{1}{2}\frac{\partial^2 U_{tot}}{\partial x_i \partial x_{i-1}} & \frac{1}{2}\frac{\partial^2 U_{tot}}{\partial x_i \partial x_{i+1}} & \frac{1}{2}\frac{\partial^2 U_{tot}}{\partial x_i \partial x_{i+2}} \\ \frac{1}{2}\frac{\partial^2 U_{tot}}{\partial x_i \partial x_{i-2}} & 0 & 0 & 0 & 0 \\ \frac{1}{2}\frac{\partial^2 U_{tot}}{\partial x_i \partial x_{i-1}} & 0 & 0 & 0 & 0 \\ \frac{1}{2}\frac{\partial^2 U_{tot}}{\partial x_i \partial x_{i+1}} & 0 & 0 & 0 & 0 \\ \frac{1}{2}\frac{\partial^2 U_{tot}}{\partial x_i \partial x_{i+2}} & 0 & 0 & 0 & 0 \end{bmatrix} \begin{bmatrix} u_i \\ u_{i-2} \\ u_{i-1} \\ u_{i+1} \\ u_{i+2} \end{bmatrix} = \begin{bmatrix} \overline{F_i} - \frac{\partial U_{tot}}{\partial x_i} \\ 0 \\ 0 \\ 0 \\ 0 \end{bmatrix} \tag{3.20}$$

The element stiffness matrix and the local force vector given in Equation 3.20 are different from the standard finite element method designed to focus on one element. Instead, the AFEM can consider the multi-body interatomic potential by focusing on the node i in Figure 3.2. It expands the factors in the stiffness matrix to the nodes i-2 and i+2 in Equation 3.17. Thus, u_{i-2} and u_{i+2} in the displacement vector influence on $\overline{F_i} - \partial U_{tot} / \partial x_i$ in the nonequilibrium force vector (Liu et al. 2003). The three-dimensional stiffness matrix and the nonequilibrium force vector for the multibody potential will be introduced in Chapter 4.

Chapter 4 AFEM Simulation

4.1 Introduction

The purpose of this chapter is to investigate the formulation of AFEM and its potential application in geo-materials such as soils and rocks. In this regard, the AFEM was validated by comparing results with one-dimensional molecular dynamics simulation. Then, the computational speed of AFEM was investigated in one and two dimensions. The mechanically strong carbon nanotube used as semiconductor was simulated so that the mechanical properties can be examined. Finally, the quartz mineral was analyzed with certain assumptions.

4.2 Molecular Dynamics and AFEM in One Dimension

4.2.1 Molecular Dynamics in One Dimension

Molecular Dynamics (MD) has been traditionally used by scientists and engineers. It is a standard method for computational nano-mechanics. In order to validate AFEM, it is important to compare the stress-strain behavior between AFEM and MD. A simple AFEM and MD simulation as performed using four atoms subjected to the same external forces. The following is the MD simulation procedure. In one-dimensional MD, Lennard-Jones potential was employed between particles and its formulas are,

$$m\ddot{x}_1 = f_{ext}^1 - 24 \cdot \varepsilon \cdot \sum_{j=2}^{4} \left(\frac{2}{(x_1 - x_j)^{13}} - \frac{1}{(x_1 - x_j)^7} \right) \tag{4.1}$$

$$m\ddot{x}_2 = f_{ext}^2 - 24 \cdot \varepsilon \cdot \sum_{\substack{j=1 \\ j \neq 2}}^{4} \left(\frac{2}{(x_2 - x_j)^{13}} - \frac{1}{(x_2 - x_j)^7} \right) \tag{4.2}$$

$$m\ddot{x}_3 = f_{ext}^3 - 24 \cdot \varepsilon \cdot \sum_{\substack{j=1 \\ j \neq 3}}^{4} \left(\frac{2}{(x_3 - x_j)^{13}} - \frac{1}{(x_3 - x_j)^7} \right) \tag{4.3}$$

$$m\ddot{x}_4 = f_{ext}^4 - 24 \cdot \varepsilon \cdot \sum_{\substack{j=1 \\ j \neq 4}}^{4} \left(\frac{2}{(x_4 - x_j)^{13}} - \frac{1}{(x_4 - x_j)^7} \right) \tag{4.4}$$

where $\ddot{x}$ is the acceleration, and f^i_{ext} is the external force exerted on atom i. ε in Equation 4.1 to 4.4 takes the value of one. The external forces f^1_{ext} and f^4_{ext} were used for extension and compression, and f^2_{ext} and f^3_{ext} were set to zero. The initial velocity was assumed to be zero, and the initial locations of atoms were set such that a distance of 1.12 Å exists between particles. The time interval was set to be 0.001, the number of iteration for MD simulation was 80000, and the mass of each particle is assumed to be one. These assumptions might be appropriate for practical purpose (Fosdick, 1995).

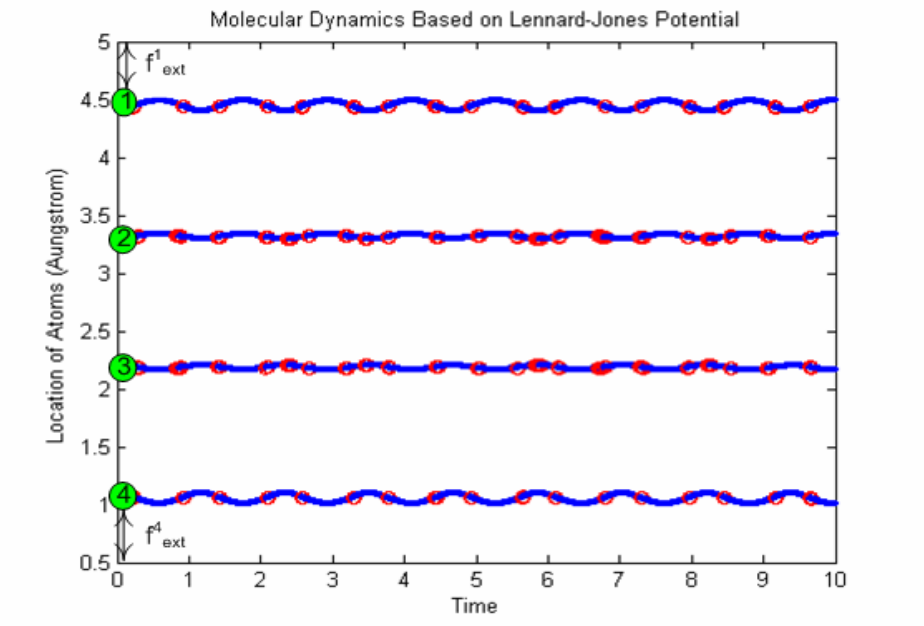

Figure 4.1 - One-dimensional MD Simulation

Figure 4.1 shows the general behavior of atoms in MD simulation which vibrate due to the interaction between atoms. The red circles on the atom path stand for the location of atoms when the sum of external and internal force becomes zero. Those atomic positions were averaged for calculating atomic deformations against external forces.

The initial condition is related to the amplitude of the vibrating atoms. For instance, the higher the initial velocity, or the more distant the initial location from the equilibrium positions, the bigger the amplitude of vibration of atoms. The time step and the mass of particles influence the efficiency and accuracy of MD. If the time step is too small, it will consume more time, resulting in decreasing computational efficiency. On the contrary, a larger time step impairs the accuracy of MD simulation. Therefore, it is required to select an appropriate time step satisfying both the efficiency and the accuracy of MD simulation.

4.2.2 Framework of One-dimensional AFEM Using Pair Potential

AFEM starts with constructing the stiffness matrix and the nonequilibrium force vector. The nonequilibrium force vector is composed of internal and external force vector. The framework of AFEM is the same as that of the finite element method based on the axial forces acting on nodes. In AFEM, the internal force vector should be calculated in the same way as how the stiffness matrix is computed in the finite element method. This is due to the nature of the internal force vector which depends on the distance between particles. The local stiffness matrix and internal force vector for the pair potential on the element connecting node i-1 and node i is,

$$\begin{bmatrix} \dfrac{\partial^2 U_{i-1,i}}{\partial x_{i-1}\partial x_{i-1}} & \dfrac{\partial^2 U_{i-1,i}}{\partial x_{i-1}\partial x_i} \\ \dfrac{\partial U^2{}_{i-1,i}}{\partial x_i \partial x_{i-1}} & \dfrac{\partial^2 U_{i-1,i}}{\partial x_i \partial x_i} \end{bmatrix} \begin{bmatrix} u_{i-1} \\ u_i \end{bmatrix} = \begin{bmatrix} -\dfrac{\partial U_{i-1,i}}{\partial x_{i-1}} \\ -\dfrac{\partial U_{i-1,i}}{\partial x_i} \end{bmatrix} \tag{4.5}$$

The right hand side of Equation 4.5 is the internal force vector. The externally applied forces can be added to the corresponding locations in the internal force vector. The stiffness matrix and the force vector require no transformation matrix with the use of the gradient operator. It automatically generates the stiffness matrix, and the internal force vector. Through iteration, the system of AFEM converges to the equilibrium state by minimizing the energy.

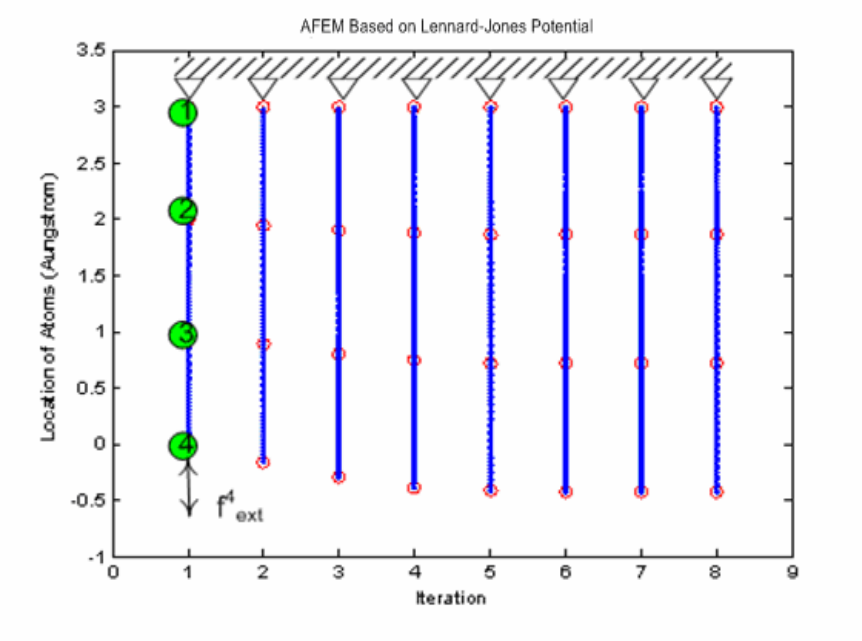

Figure 4.2 - One-dimensional AFEM Simulation

Equivalent to the MD system in Figure 4.1, the AFEM model was prepared, as illustrated in Figure 4.2. The boundary condition set on atom #1 was a constraint. The external force placed on atom #4 is the same as the force applied on atom #4 in Figure 4.1, but the external force on atom #1 in MD simulation was replaced by the reaction force in the AFEM simulation. After atom #4 was displaced in Figure 4.2, the system motion stopped at the 8th iteration. The displacements in AFEM simulation are usually the largest at the first iteration, and decrease as the iterations continue, finally approaching zero.

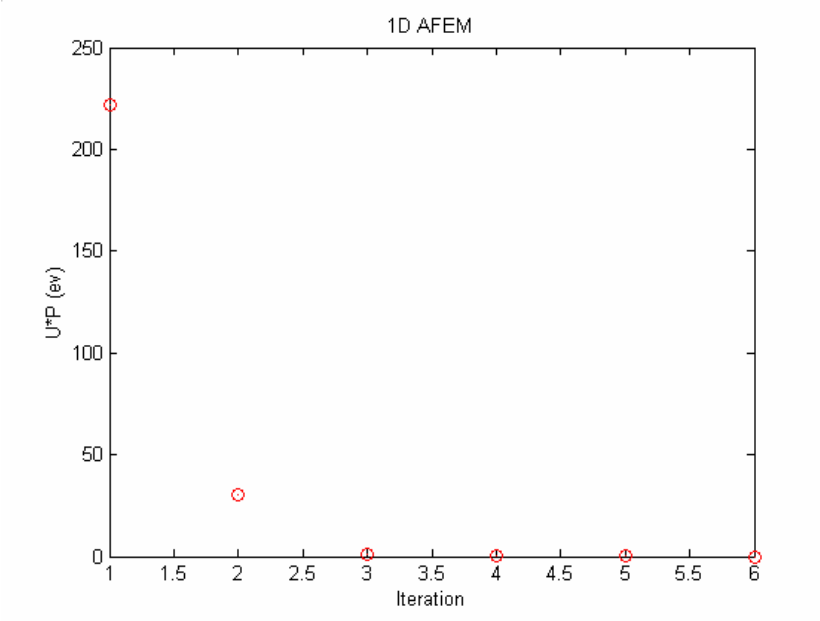

Figure 4.3 - U'·P with Iteration

One way to check the convergence of AFEM system is to estimate U'·P at every iteration step as shown in Figure 4.3. U is the displacement vector, and P is the nonequilibrium force vector. U and P share the same sign since the direction of forces should agree with the direction of deformations. Therefore, the dot product of U and P vector should be positive. The deformation during iteration should be smaller and smaller. Thus, the dot product of U and P vector should be decreased at every iteration step. However, it should be noted that some of values in P vector may increase, especially at the second iteration. Therefore, it is more desirable to observe the dot product of U and P vector rather than P vector.

4.2.3 Comparison between AFEM and MD Simulation

The displacements due to external forces were calculated using the AFEM and MD simulations and were listed in Table 4.1. The unit of Lennard-Jones potential energy and length used in this simulation are electric volt (ev) and Angstrom (Å), respectively.

Table 4.1 - Distance between Atoms after Minimizing Energy

External Force (ev/Å)	Method	First-Second (Å)	Second-Third (Å)	Third-Fourth (Å)	Total Length (Å)
-0.6	AFEM	1.13240	1.13078	1.13240	3.39557
-0.6	MD	1.13206	1.13120	1.13206	3.39531
-0.4	AFEM	1.12829	1.12676	1.12829	3.38334
-0.4	MD	1.12812	1.12720	1.12807	3.38339
-0.2	AFEM	1.12449	1.12303	1.12449	3.37200
-0.2	MD	1.12453	1.12316	1.12448	3.37217
0	AFEM	1.12094	1.11954	1.12094	3.36142
0	MD	1.12094	1.11954	1.12094	3.36142
0.2	AFEM	1.11761	1.11627	1.11761	3.35149
0.2	MD	1.11763	1.11633	1.11764	3.35159
0.4	AFEM	1.11448	1.11318	1.11448	3.34214
0.4	MD	1.11448	1.11315	1.11447	3.34210
0.6	AFEM	1.11151	1.11027	1.11151	3.33329
0.6	MD	1.11164	1.10986	1.11160	3.33311

.

In Table 4.1, the total length refers to the distance between the first atom and the fourth atom. The difference observed in the two systems was plotted in Figure 4.4. A good agreement between the two methods is observed, even for the maximum difference of displacement of 0.00026 Å, which is relatively small, considering that the total length of both systems is 3.38 Å on average.

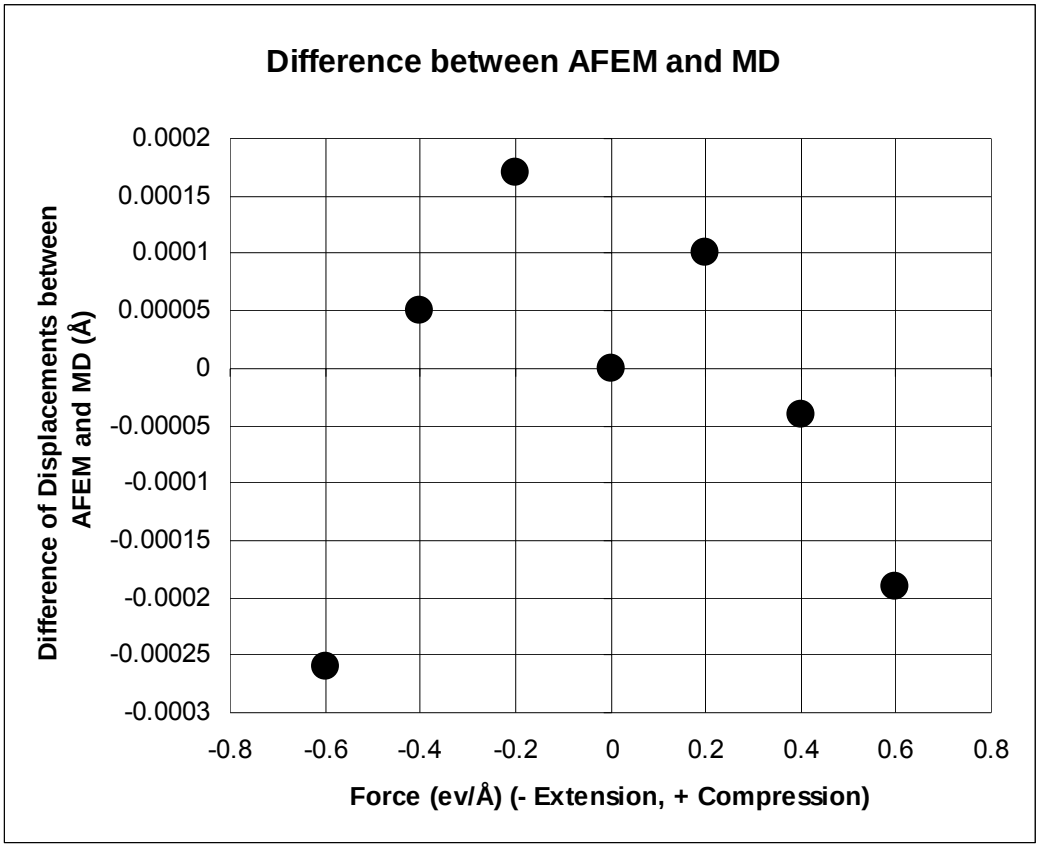

Figure 4.4 - Disagreement of Displacements between AFEM and MD

During MD simulation, the error generated per time step will accumulate to cause mistakes. Furthermore, MD might give a slightly different result, depending on the method selected to estimate the distance between particles due to the vibrating nature of the MD simulation. In this MD simulation, the position of atoms was determined when the acceleration of each atom becomes zero. There might not be enough points exactly satisfying the acceleration to be zero since atoms moves with a finite time step. Alternatively, the coordinates of atoms were collected and averaged if their forces are less than 0.1 ev/ Å and more than -0.1 ev/ Å.

4.2.4 Theoretical Comparison between AFEM and MD

Analysis of AFEM and MD shows similarity between the two methods. Let us discuss the theory of both methods. The main idea of AFEM is to make the non-equilibrium force vector zero. That is,

$$\sum F_i = f_i - \frac{\partial U}{\partial x_i} = 0 \tag{4.6}$$

The governing Equations 4.1 to 4.4 for MD suggest that the system would be in equilibrium if forces between atoms are zero. This can be expressed as,

$$\sum F_i = m_i \ddot{x}_i = f_i - \frac{\partial U}{\partial x_i} = 0 \tag{4.7}$$

where the ΣF_i is the difference between the internal and external forces acting on atom i, f_i is the externally applied force, and $\partial U / \partial x_i$ is the internal force. In short, Equation 4.6 and 4.7 are the same. It suggests that the AFEM and MD share the same framework. Both systems start with arbitrary locations and allow atoms to move toward the equilibrium positions. The difference between the AFEM and MD depends on how they reach the equilibrium state.

MD updates the locations of atoms within every tiny time step. With time, each atom moves towards its equilibrium position, and the force relaxation takes place. The system evolves from the nonequilibrium to the equilibrium state. However, AFEM employs the stiffness matrix composed of gradients. The stiffness matrix indicates the direction of atoms to move in order to arrive at the equilibrium state. Therefore, AFEM gathers all atoms in the system, and send them to the minimal energy state.

4.2.5 Vectorization and Sparse Matrix Calculations

AFEM was programmed in MATLAB which is specifically suited for numerical computation with matrixes and vectors. There are two methods in Matlab to save the computational time. The simulation of discrete atoms in AFEM requires the computation of electric forces between atoms. Since each element can be independently computed, the vectorizing algorithm can significantly save the computational time. At this point, it is necessary to give an example to explain the vectorization scheme. If there are x values ranging from 0 to 100, increasing by a step of 0.01, the function of the product between sin(x) by cos(x) can be completed using the following codes.

```
i = 0;
for x = 0:0.01:100
i = i + 1;
y(i) = sin(x) * cos(x);
end
```

It requires 10000 times the iterations for calculating the individual x values. However, the vectorization transforms all x values stored as a form of a vector to another y vector. Using vectorization scheme, a much simpler and timesaving code can be expressed as,

```
x = 0:0.01:100;
y= sin(x).* cos(x);
```

It turns out that the vectorization code given above is amazingly 45 times faster than the 'for' loop. The vectorization in MATLAB based on the vector multiplication can evaluate the electric forces faster after all necessary inputs such as the node numbers and coordinates of atoms are organized as vectors.

Another important feature of MATLAB is the sparse command. The stiffness matrix used in AFEM is typically sparse, and inverting a sparse stiffness matrix takes less time than a matrix filled with more components. It is necessary to make MATLAB software recognize a sparse matrix whose transformation can be written as S=sparse(K). K is the stiffness matrix desired to be transformed into the sparse matrix, and S is the sparse matrix. The sparse command eliminates zero components in the stiffness matrix, resulting in a big saving of computer memory.

4.2.6 Speed of One-dimensional AFEM

In order to check the speed of one dimensional AFEM, different numbers of atoms in the AFEM system were simulated. The Lennard-Jones pair potential was employed between atoms. At this time, it was assumed that the potential in one atom is only affected by the nearest neighboring atoms. As a boundary condition, the atom at one end was fixed, and the other side was displaced by the external force of 1.5 ev/Å. In addition, the distance between atoms is initially set to be 1.1 Å which is close to the equilibrium distance of 1.1225 Å.

Table 4.2 - Computational Time in One-dimensional AFEM

Number of Atoms	Iteration	Time Used for Computing Elements (Second)	Time Used for Inverting K Matrix (Second)	Total Computation Time (Second)
100	6	0.016	0.000	0.016
400	6	0.079	0.031	0.110
800	6	0.156	0.094	0.250
1200	6	0.265	0.188	0.453
1600	6	0.422	0.313	0.735
2000	6	0.608	0.454	1.062
2400	6	0.829	0.640	1.469
2800	6	1.077	0.845	1.922
3200	6	1.358	1.095	2.453
3600	6	1.640	1.360	3.000
4000	6	2.077	1.641	3.718

Again, the computation time of AFEM mainly consists of two stages. The first is to calculate the element properties for preparing the stiffness matrix and nonequilibrium force vector. This process was named 'computing elements' in Table 4.2 and Figure 4.5. The next step is to invert the K matrix to calculate displacements. Then, the iteration process continues until the nonequilibrium force vector goes to zero.

Table 4.2 shows how long AFEM takes at each stage. The number of atoms varies from 100 to 4000, and the computation time was estimated until the maximum value of the P vector is less than 10^{-11} ev/Å. The inverse of K matrix approximately takes 43 % of the total computation time. In order to invert the stiffness matrix in the AFEM simulation, MATLAB uses the Gaussian elimination.

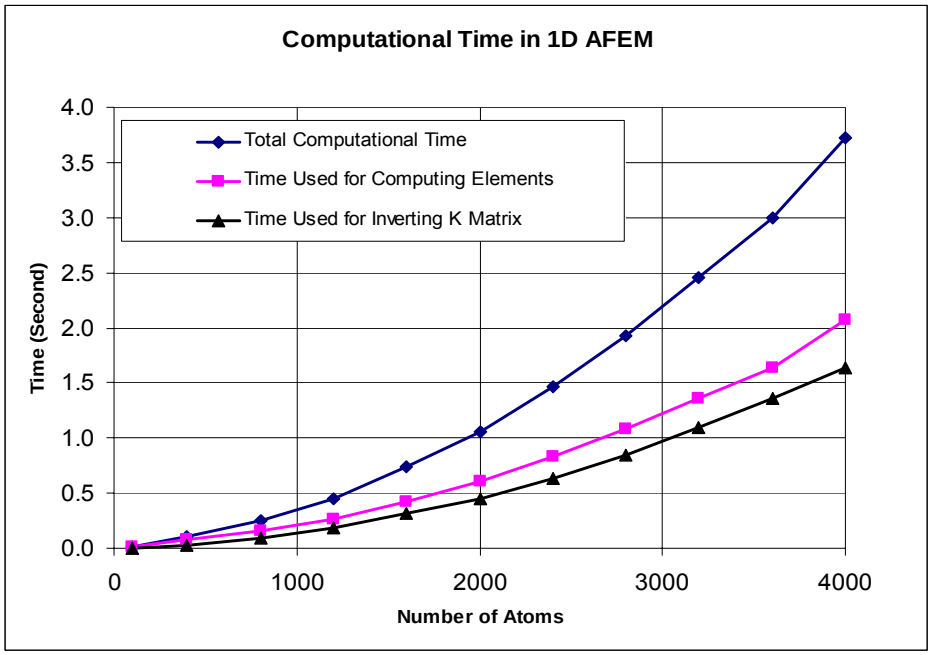

Figure 4.5 - Computation Time in One-dimensional AFEM

The vectorization and the sparse command in MATLAB environment significantly saved computation time. For example, in Figure 4.5, even 4000 atoms in a one-dimensional AFEM simulation can be computed in less than 4 seconds. However, time used for

analyzing elements and inverting the stiffness matrix is not exactly proportional to the number of atoms while the literature of Atomic-scale finite element method reports that the computation time in the AFEM is proportional to the number of atoms, O(N) (Liu et al. 2004). The computation time will be discussed in detail at the end of 2D AFEM simulation.

4.3 AFEM in Two Dimensions

4.3.1 Framework of Two-dimensional AFEM Using Pair Potential

In the two-dimensional AFEM, the atom has one more degree of freedom than in the one-dimensional AFEM. The stiffness matrix and the non-equilibrium force vector for the pair potential in the two-dimensional AFEM is,

$$\begin{bmatrix} \frac{\partial^2 U_{i-1,i}}{\partial x_{i-1}\partial x_{i-1}} & \frac{\partial^2 U_{i-1,i}}{\partial x_{i-1}\partial y_{i-1}} & \frac{\partial^2 U_{i-1,i}}{\partial x_{i-1}\partial x_i} & \frac{\partial^2 U_{i-1,i}}{\partial x_{i-1}\partial y_i} \\ \frac{\partial^2 U_{i-1,i}}{\partial y_{i-1}\partial x_{i-1}} & \frac{\partial^2 U_{i-1,i}}{\partial y_{i-1}\partial y_{i-1}} & \frac{\partial^2 U_{i-1,i}}{\partial y_{i-1}\partial x_i} & \frac{\partial^2 U_{i-1,i}}{\partial y_{i-1}\partial y_i} \\ \frac{\partial^2 U_{i-1,i}}{\partial x_i\partial x_{i-1}} & \frac{\partial^2 U_{i-1,i}}{\partial x_i\partial y_{i-1}} & \frac{\partial^2 U_{i-1,i}}{\partial x_i\partial x_i} & \frac{\partial^2 U_{i-1,i}}{\partial x_i\partial y_i} \\ \frac{\partial^2 U_{i-1,i}}{\partial y_i\partial x_{i-1}} & \frac{\partial^2 U_{i-1,i}}{\partial y_i\partial y_{i-1}} & \frac{\partial^2 U_{i-1,i}}{\partial y_i\partial x_i} & \frac{\partial^2 U_{i-1,i}}{\partial y_i\partial y_i} \end{bmatrix} \begin{bmatrix} u_{x(i-1)} \\ u_{y(i-1)} \\ u_{x(i)} \\ u_{y(i)} \end{bmatrix} = \begin{bmatrix} -\frac{\partial U_{i-1,i}}{\partial x_{i-1}} \\ -\frac{\partial U_{i-1,i}}{\partial y_{i-1}} \\ -\frac{\partial U_{i-1,i}}{\partial x_i} \\ -\frac{\partial U_{i-1,i}}{\partial y_i} \end{bmatrix} \tag{4.8}$$

The stiffness matrix is symmetric. The externally applied force has been omitted in the nonequilibrium force vector. In the two-dimensional AFEM, the external forces can be added in the nonequilibrium force vector after the construction of the internal force vector is completed.

4.3.2 Details of Two-dimensional AFEM

As in the one-dimensional AFEM simulation, a different number of atoms has been prepared for checking the speed. Two-dimensional AFEM meshes have 100, 400, 900, 1600, 2025 and 2500 atoms. The structures are all squares, and individual atoms are arranged in a triangular fashion. In each system, external forces are applied on the four nodes on the top of the structure. The magnitude of each external force is 9 ev/Å, and its direction is towards the bottom so that the structure is compressed. The locations where the forces are applied were marked with red, as illustrated from Figure 4.5 to 4.10. Each system was simulated until the maximal absolute value in the non-equilibrium vector becomes less than 10^{-10} ev/Å.

The boundary condition was set at the bottom of the structure in the same way as the finite element method. Every node at the bottom has a roller so that atoms at the bottom of the structure are constrained in the vertical direction. In addition, to stabilize the structure in the x direction, one of the atoms at the bottom was fixed.

The initial distance between atoms is set to be 1.1 Å which is close to the equilibrium length. It is important to note that AFEM might diverge if the initial location of atoms is set to be far from the equilibrium configuration of the structure. If the pair potential is used, the equilibrium distance can be estimated by the simple equation given by $\partial U / \partial r = 0$. It should be pointed out that the equilibrium distance is independent of the external force.

Figures 4.6 to 4.11 describe the final configurations of two-dimensional AFEM. It is interesting to observe the deformation around the locations where external forces were applied.

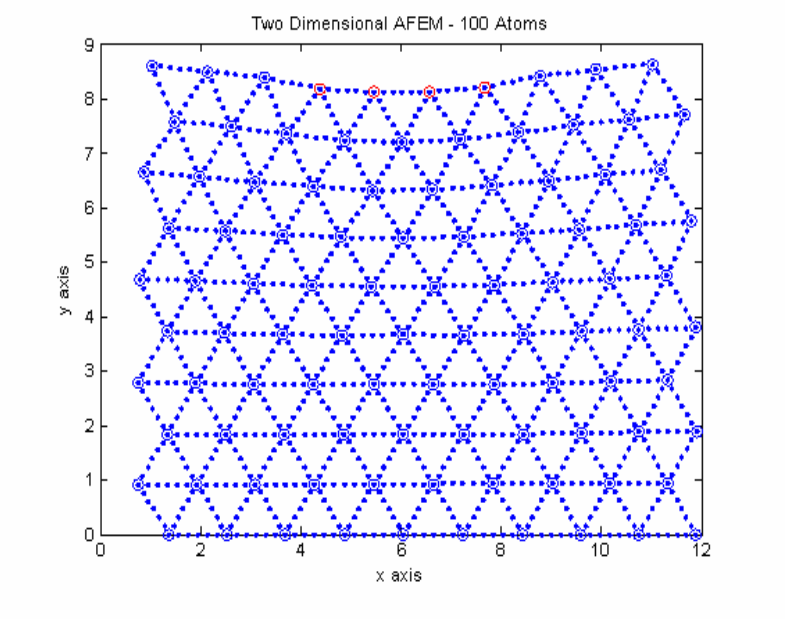

Figure 4.6 - 100 Atoms Requiring 11 Steps

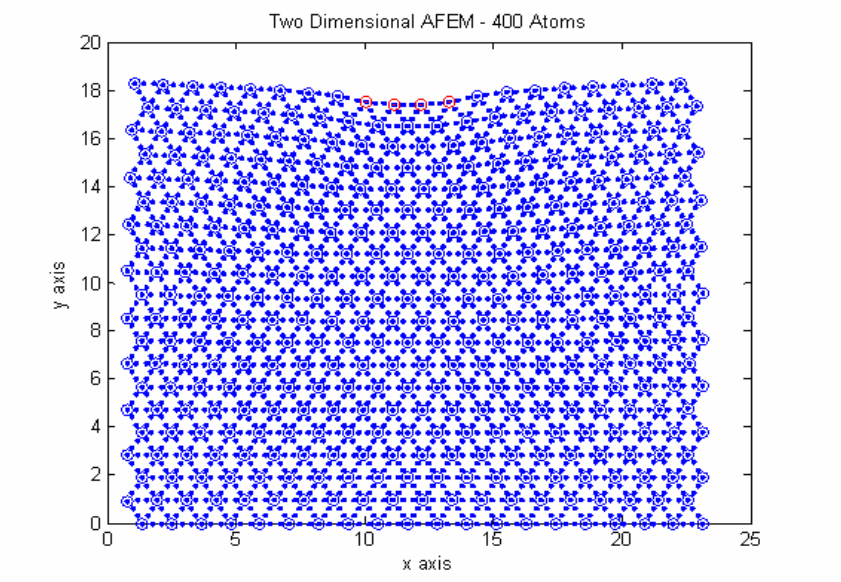

Figure 4.7 - 400 Atoms Requiring 16 Steps

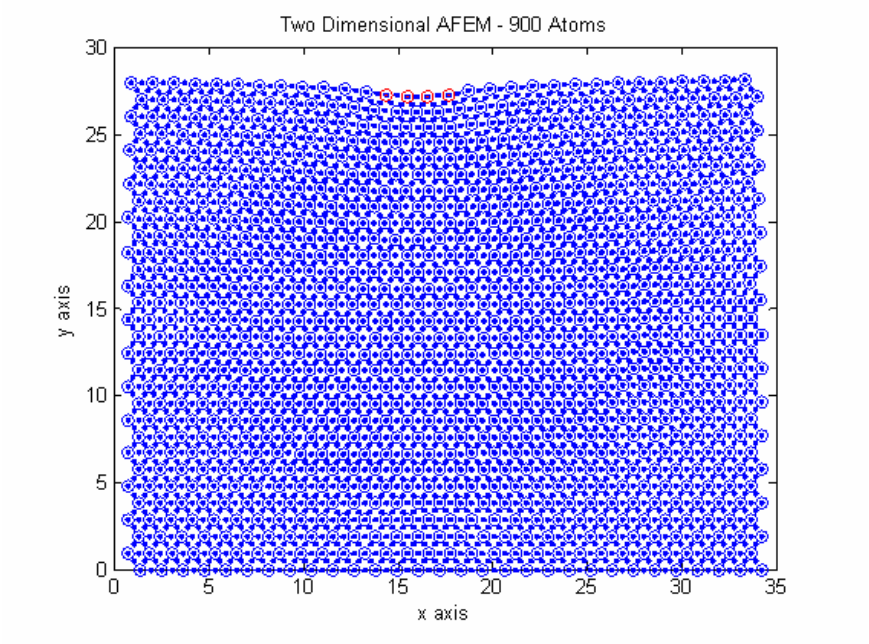

Figure 4.8 - 900 Atoms Requiring 11 Steps

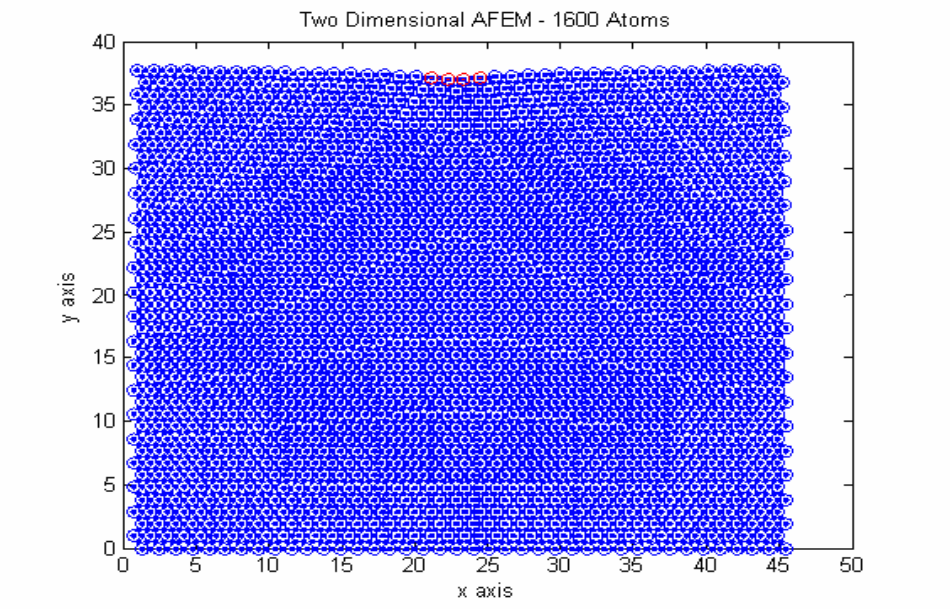

Figure 4.9 - 1600 Atoms Requiring 9 Steps

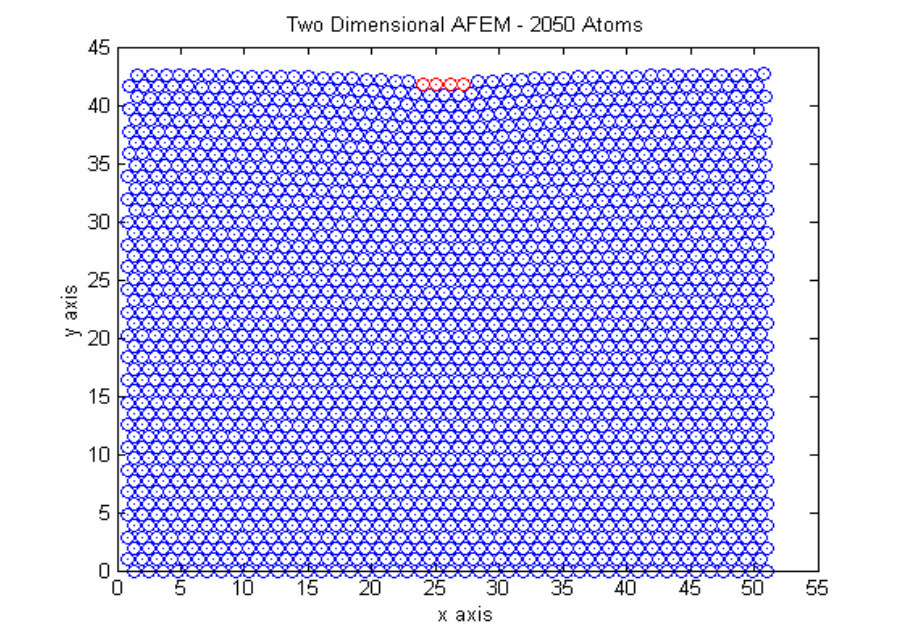

Figure 4.10 - 2025 Atoms Requiring 12 Steps

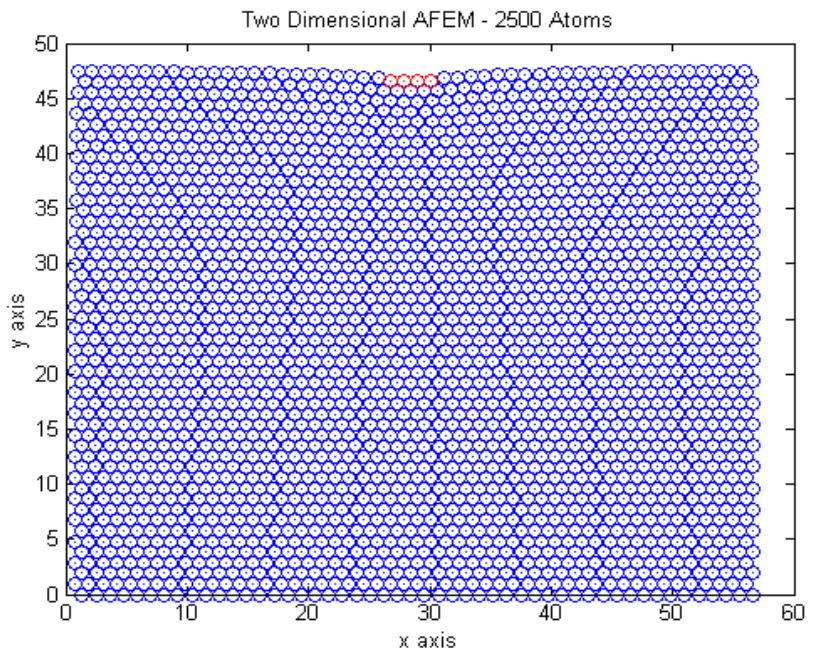

Figure 4.11 - 2500 Atoms Requiring 12 Steps

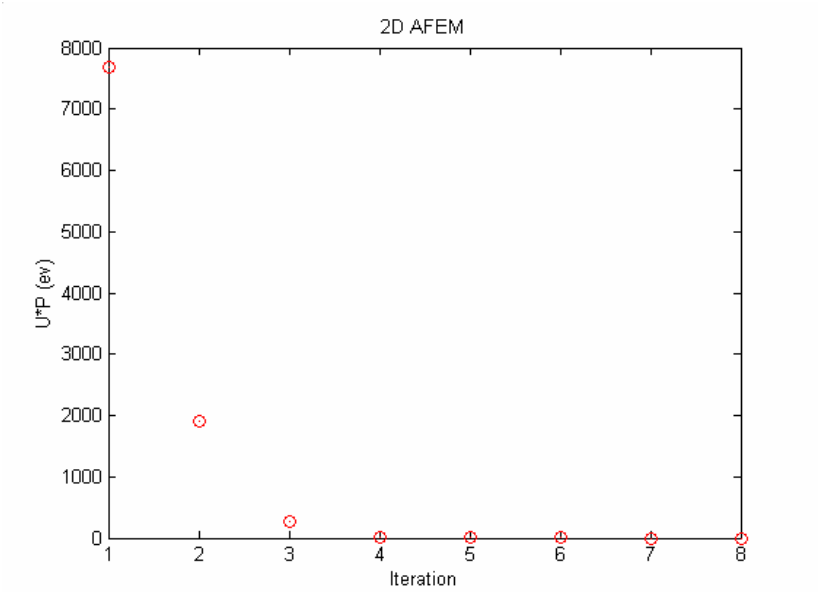

Figure 4.12 - U'·P with Iteration

As was discussed in Figure 4.3, the dot product of U and P vector converges as the iteration proceeds. Again, this value should be positive and become smaller as iteration proceeds.

4.3.3 Speed of Two-dimensional AFEM

Table 4.3 - Computational Time in Two-dimensional AFEM

Number of Atoms	Iteration	Time Used for Computing Elements (Second)	Time Used for Inverting K Matrix (Second)	Total Computation Time (Second)
100	11	0.436	0.064	0.500
400	16	1.422	0.348	1.770
900	11	3.977	0.793	4.770
1600	9	7.458	1.422	8.880
2025	12	10.086	4.484	14.570
2500	12	39.204	8.796	48.000

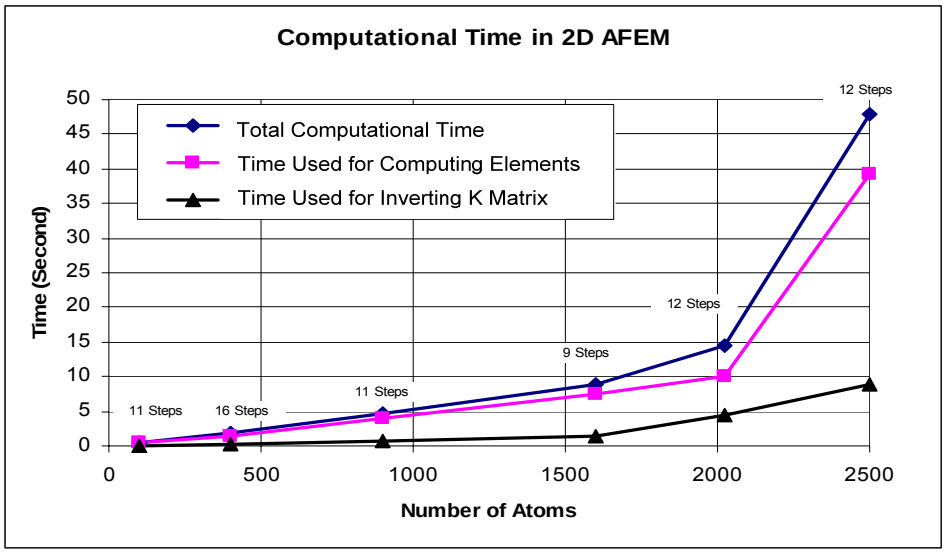

Figure 4.13 - Computational Time in Two-dimensional AFEM

The results of the computational times of two-dimensional AFEM are tabulated in Table 4.3 and illustrated in Figure 4.13. Figure 4.13 shows that the computational time of two-dimensional AFEM is non-linear to the number of atoms, and time used for computing element properties and inverting the stiffness matrix is also not proportional to the number of atoms, O(N)

The computation time significantly increases if more than 2000 atoms are involved in 2D AFEM. In particular, in the 2500 atomic system, the computational time for calculating element properties contributed significantly to the time consumption which prevents the system from becoming O(N). It is possible that the vectorization is not effective if the size of vector is large in MATLAB. For example, the sizes of vectors used in the 2025 and 2500 atomic system are 5896 by 1 and 7301 by 1, respectively. However, Figure 4.13 indicates that the computation time is approximately proportional to the number of atoms, O(N), only when N<2000.

ABAQUS software had been adopted in the previous study by Liu (2003) while MATLAB was used in this study. It is possible that the different characteristic between ABAQUS and

MATLAB might give a different result. At this point, it is recommended to simulate AFEM with FORTRAN or C Language to follow their AFEM speed.

4.4 AFEM in Three Dimensions – Single Walled Carbon Nanotube

4.4.1 Structure of Carbon Nanotube Using Multibody Potential

In this section, the three-dimensional AFEM will be discussed. A representative example is the single walled carbon nano-tube (CNT). The CNT has a hexagonal lattice structure. A part of (7,7) armchair CNT is described in Figure 4.14.

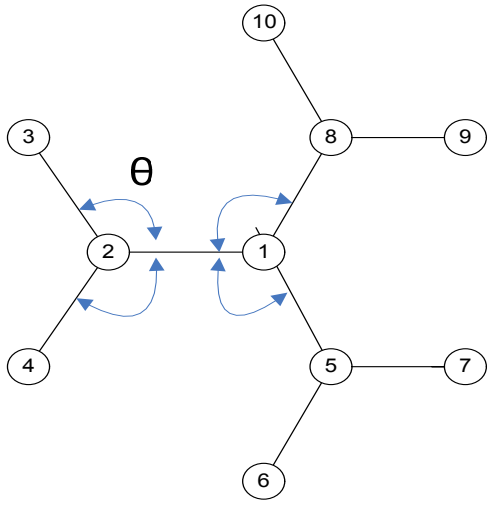

Figure 4.14 - Part of (7, 7) Armchair CNT Lattice Structure

Equations 2.18 to 2.24 explaining the Tersoff-Brenner potential are used for analyzing the CNT. Figure 4.14 shows how Tersoff-Brenner potential works on CNT. It has a multibody nature. For example, in Figure 4.14, the energy stored on atom #1 changes when the nearest neighboring atoms # 2, 5 and 8 as well as the second nearest atoms # 3, 4, 6, 7, 9, and 10

are displaced. The second nearest atoms are connected through the angle bending. The angles made by the element 1-2 and its neighbor elements such as 2-3, 2-4, 1-5 and 1-8 are used for angle bending. In fact, the angle can be expressed with the bond stretching term. For instance, if θ is the angle between element 2-1 and 2-3 and the length of an element i-j is defined as $\overline{i,j}$, then

$$\cos(\theta) = \frac{\overline{1,2}^2 + \overline{2,3}^2 - \overline{1,3}^2}{2 \cdot \overline{1,2} \cdot \overline{2,3}} \tag{4.9}$$

Therefore, the angle bending θ can be calculated using the bond stretching with elements 1-2, 2-3 and 1-3 which is a function of the location of atom #1 and the second-nearest atom #3. It is usually designed to keep a specific angle against externally applied forces, and at the same time, it confines the distance from one atom and its second nearest atoms. In other words, the invisible bond stretching terms between atom #1 and its second nearest atoms #3, 4, 6, 7, 9 and 10 are implicitly assumed through the angle bending. This mechanism makes it possible to achieve the stability of CNT.

4.4.2 Framework of Three-dimensional AFEM for CNT

The stiffness matrix and the nonequilibrium force vector focused on atom #1 in Figure 4.14 have a form of,

$$\begin{bmatrix} \left(\dfrac{\partial^2 U_{tot}}{\partial x_1 \partial x_1}\right)_{3\times 3} & \left(\dfrac{1}{2}\dfrac{\partial^2 U_{tot}}{\partial x_1 \partial x_i}\right)_{3\times 27} \\ \left(\dfrac{1}{2}\dfrac{\partial^2 U_{tot}}{\partial x_i \partial x_1}\right)_{27\times 3} & (0)_{27\times 27} \end{bmatrix} \begin{bmatrix} (u_1)_{3\times 1} \\ (u_i)_{27\times 1} \end{bmatrix} = \begin{bmatrix} \left(\overline{F}_1 - \dfrac{\partial U_{tot}}{\partial x_1}\right)_{3\times 1} \\ (0)_{27\times 1} \end{bmatrix} \tag{4.10}$$

The stiffness matrix of Equation 4.10 was given by B. Liu et al. The Atom # i indicates atoms from #2 to 10 located around the atom #1 in Figure 4.14. The explicit framework of 30 by 30 stiffness matrix is given by,

$$\begin{bmatrix}
\frac{\partial^2 U_{tot}}{\partial x_1 \partial x_1} & \frac{\partial^2 U_{tot}}{\partial x_1 \partial y_1} & \frac{\partial^2 U_{tot}}{\partial x_1 \partial z_1} & \frac{1}{2}\frac{\partial^2 U_{tot}}{\partial x_1 \partial x_2} & \frac{1}{2}\frac{\partial^2 U_{tot}}{\partial x_1 \partial y_2} & \frac{1}{2}\frac{\partial^2 U_{tot}}{\partial x_1 \partial z_2} & \cdots & \frac{1}{2}\frac{\partial^2 U_{tot}}{\partial x_1 \partial x_{10}} & \frac{1}{2}\frac{\partial^2 U_{tot}}{\partial x_1 \partial y_{10}} & \frac{1}{2}\frac{\partial^2 U_{tot}}{\partial x_1 \partial z_{10}} \\
\frac{\partial^2 U_{tot}}{\partial y_1 \partial x_1} & \frac{\partial^2 U_{tot}}{\partial y_1 \partial y_1} & \frac{\partial^2 U_{tot}}{\partial y_1 \partial z_1} & \frac{1}{2}\frac{\partial^2 U_{tot}}{\partial y_1 \partial x_2} & \frac{1}{2}\frac{\partial^2 U_{tot}}{\partial y_1 \partial y_2} & \frac{1}{2}\frac{\partial^2 U_{tot}}{\partial y_1 \partial z_2} & \cdots & \frac{1}{2}\frac{\partial^2 U_{tot}}{\partial y_1 \partial x_{10}} & \frac{1}{2}\frac{\partial^2 U_{tot}}{\partial y_1 \partial y_{10}} & \frac{1}{2}\frac{\partial^2 U_{tot}}{\partial y_1 \partial z_{10}} \\
\frac{\partial^2 U_{tot}}{\partial z_1 \partial x_1} & \frac{\partial^2 U_{tot}}{\partial z_1 \partial y_1} & \frac{\partial^2 U_{tot}}{\partial z_1 \partial z_1} & \frac{1}{2}\frac{\partial^2 U_{tot}}{\partial z_1 \partial x_2} & \frac{1}{2}\frac{\partial^2 U_{tot}}{\partial z_1 \partial y_2} & \frac{1}{2}\frac{\partial^2 U_{tot}}{\partial z_1 \partial z_2} & \cdots & \frac{1}{2}\frac{\partial^2 U_{tot}}{\partial z_1 \partial x_{10}} & \frac{1}{2}\frac{\partial^2 U_{tot}}{\partial z_1 \partial y_{10}} & \frac{1}{2}\frac{\partial^2 U_{tot}}{\partial z_1 \partial z_{10}} \\
\frac{1}{2}\frac{\partial^2 U_{tot}}{\partial x_1 \partial x_2} & \frac{1}{2}\frac{\partial^2 U_{tot}}{\partial y_1 \partial x_2} & \frac{1}{2}\frac{\partial^2 U_{tot}}{\partial z_1 \partial x_2} & 0 & 0 & 0 & \cdots & 0 & 0 & 0 \\
\frac{1}{2}\frac{\partial^2 U_{tot}}{\partial x_1 \partial y_2} & \frac{1}{2}\frac{\partial^2 U_{tot}}{\partial y_1 \partial y_2} & \frac{1}{2}\frac{\partial^2 U_{tot}}{\partial z_1 \partial y_2} & 0 & 0 & 0 & \cdots & 0 & 0 & 0 \\
\frac{1}{2}\frac{\partial^2 U_{tot}}{\partial x_1 \partial z_2} & \frac{1}{2}\frac{\partial^2 U_{tot}}{\partial y_1 \partial z_2} & \frac{1}{2}\frac{\partial^2 U_{tot}}{\partial z_1 \partial z_2} & 0 & 0 & 0 & \cdots & 0 & 0 & 0 \\
\vdots & \vdots & \vdots & \vdots & \vdots & \vdots & \ddots & \vdots & \vdots & \vdots \\
\frac{1}{2}\frac{\partial^2 U_{tot}}{\partial x_1 \partial x_{10}} & \frac{1}{2}\frac{\partial^2 U_{tot}}{\partial y_1 \partial x_{10}} & \frac{1}{2}\frac{\partial^2 U_{tot}}{\partial z_1 \partial x_{10}} & 0 & 0 & 0 & \cdots & 0 & 0 & 0 \\
\frac{1}{2}\frac{\partial^2 U_{tot}}{\partial x_1 \partial y_{10}} & \frac{1}{2}\frac{\partial^2 U_{tot}}{\partial y_1 \partial y_{10}} & \frac{1}{2}\frac{\partial^2 U_{tot}}{\partial z_1 \partial y_{10}} & 0 & 0 & 0 & \cdots & 0 & 0 & 0 \\
\frac{1}{2}\frac{\partial^2 U_{tot}}{\partial x_1 \partial z_{10}} & \frac{1}{2}\frac{\partial^2 U_{tot}}{\partial y_1 \partial z_{10}} & \frac{1}{2}\frac{\partial^2 U_{tot}}{\partial z_1 \partial z_{10}} & 0 & 0 & 0 & \cdots & 0 & 0 & 0
\end{bmatrix} \tag{4.11}$$

Equation 4.11 was for the three dimensional AFEM expanded from Equation 3.20 used in one dimension. This system is used for analyzing the CNT. If the CNT has N carbon atoms, Equation 4.11 should be computed N times to construct the stiffness matrix and the corresponding nonequilibrium force vector.

U_{tot} is the sum of the Tersoff-Brenner potential energies exerted on atom # 1 written as,

$$U_{tot} = U(r_{1,2}) + U(r_{1,5}) + U(r_{1,8}) \tag{4.12}$$

where $U(r_{ij})$ is equal to $V(r_{ij})$ in Equation 2.18. Again, it is important to note that the Tersoff-Brenner potential has a multibody nature. In fact, Equation 4.12 consists of many terms when the Tersoff-Brenner potential is used. Therefore, the second derivative of Equation 4.12 with analytical solution turns out to occupy too much memory of a computer. At this time, to construct the stiffness matrix, the second derivatives should be calculated using numerical method such as,

$$\frac{\partial f(x,y,z)}{\partial x} = \frac{f(x+h,y,z) - f(x-h,y,z)}{2 \cdot h} \tag{4.13}$$

$$\frac{\partial f(x,y,z)}{\partial y} = \frac{f(x,y+h,z) - f(x,y-h,z)}{2 \cdot h} \tag{4.14}$$

$$\frac{\partial f(x,y,z)}{\partial z} = \frac{f(x,y,z+h) - f(x,y,z-h)}{2 \cdot h} \tag{4.15}$$

where

$$f(x,y,z) = \begin{cases} \dfrac{\partial U(x,y,z)_{tot}}{\partial x} \\ \dfrac{\partial U(x,y,z)_{tot}}{\partial y} \\ \dfrac{\partial U(x,y,z)_{tot}}{\partial z} \end{cases} \tag{4.16}$$

Equation 4.16 for constructing the nonequilibrium force vector can be directly derived as an analytic solution. Equations 4.13 to 4.15 provide the numerical solutions for the second derivative of energy in the stiffness matrix. The value of h in Equations 4.13 to 4.15 should be small enough to prevent error. This numerical method has an error of $O(h^2)$.

4.4.3 Boundary Condition Used for Analyzing CNT

The stiffness matrix of AFEM is symmetric, and its determinant is zero. Thus, inverting stiffness matrix requires specific boundary conditions to prevent the rigid body motion. The positions of atoms change as the AFEM system starts from the nonequilibrium to the equilibrium state. In order to arrive at the equilibrium state, it is important to construct the AFEM environment to give every atom in the system the freedom to move.

Traditionally, there are two ways to set the boundary condition in the finite element method: homogeneous boundary condition and nonhomogeneous boundary condition (Logan, 1993). The homogeneous boundary condition imposes the zero displacement on some of the nodes. It might be impossible to fix two atoms in AFEM system since the initial distance between them would make them in the nonequilibrium condition.

In the case of the nonhomogeneous boundary condition, we specify the non-zero displacement on some atoms before inverting the stiffness matrix. In AFEM, the displacements of atoms per iteration for the boundary condition may be impossible to know since they are unknown values. Thus, what should be applied to CNT are external forces, and controlling strain is not our present interest. At this point, it is desirable to create a special homogeneous boundary condition.

It is supposed that the top and bottom of the CNT will become less sensitive to horizontal deformation if axial external forces are applied. Thus, it is possible to fix atoms with springs at the top and bottom of CNT as boundary conditions. All the atoms at the top and bottom of CNT were constrained by the springs in horizontal direction.

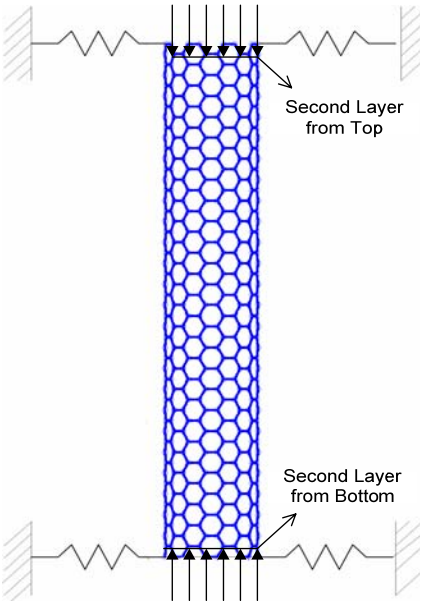

Figure 4.15 - Boundary Condition and External Forces for CNT (Side View)

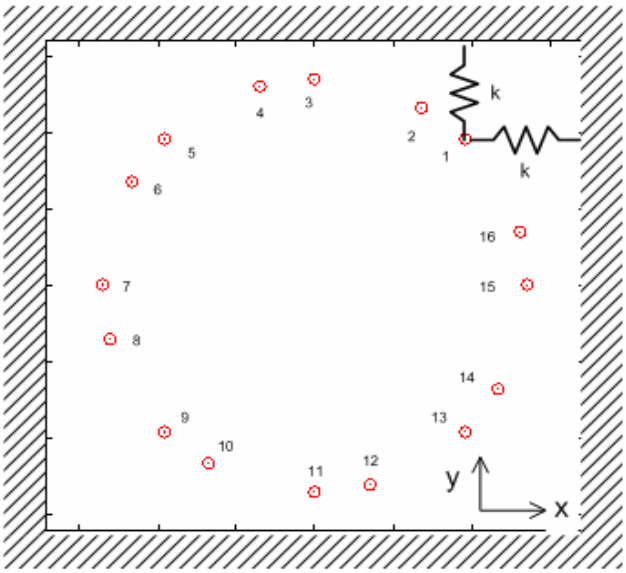

Figure 4.16 - Boundary Condition for CNT (Plan View)

The (7, 7) armchair CNT in this simulation contains 16 atoms at each layer. Figure 4.15 and 4.16 describe the way the boundary condition is applied. For example, atom #1 in Figure

4.16 is confined by the two springs oriented along the x and y axis. Likewise, all the other atoms have the same boundary condition as atom #1.

It is expected that if the stiffness of springs is larger, it would be slow for the nonequilibrium force vector acting on the atoms at the top and bottom of CNT to become zero. Through trial and error, the spring stiffness of 3000 ev/nm^2 is determined to be appropriate.

$$\text{Stiffness Matrix}=\begin{bmatrix} & \#3\cdot i-2 & \#3\cdot i-1 & \#3\cdot i & \\ \ddots & \vdots & \vdots & \vdots & \iddots \\ \cdots & k_{i,xx}+(k_{spring}) & k_{i,xy} & k_{i,xz} & \cdots \\ \cdots & k_{i,yx} & k_{i,yy}+(k_{spring}) & k_{i,yz} & \cdots \\ \cdots & k_{i,zx} & k_{i,zy} & k_{i,zz} & \cdots \\ \iddots & \vdots & \vdots & \vdots & \ddots \end{bmatrix} \begin{matrix} \\ \\ \#3\cdot i-2 \\ \#3\cdot i-1 \\ \#3\cdot i \\ \\ \end{matrix}$$

Figure 4.17 - Boundary Condition on Atom # i

The spring stiffness should be added to the global stiffness matrix. For example, the location of stiffness related to atom # i and spring boundary condition ranges from (3·i-2) to (3·i) in the global stiffness matrix as shown in Figure 4.17 since atoms are defined in three-dimensional Cartesian coordinate. Since the horizontal springs are established, the stiffness of springs in x and y direction should be added on atoms at the top and bottom of the CNT as explained in Figure 4.16.

Unfortunately, however, some non-zero values in P vector at a final stage remained on some nodes around the spring boundaries, shown in Figure 4.18, 4.19 and 4.20.

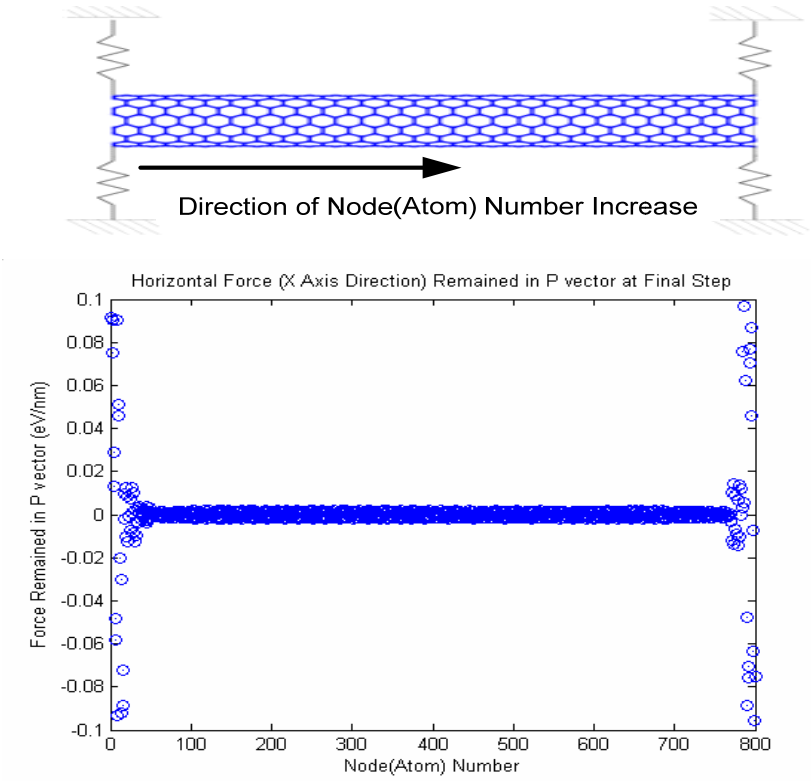

Figure 4.18 - Horizontal Forces Remained in P Vector at Final Stage (X Direction)

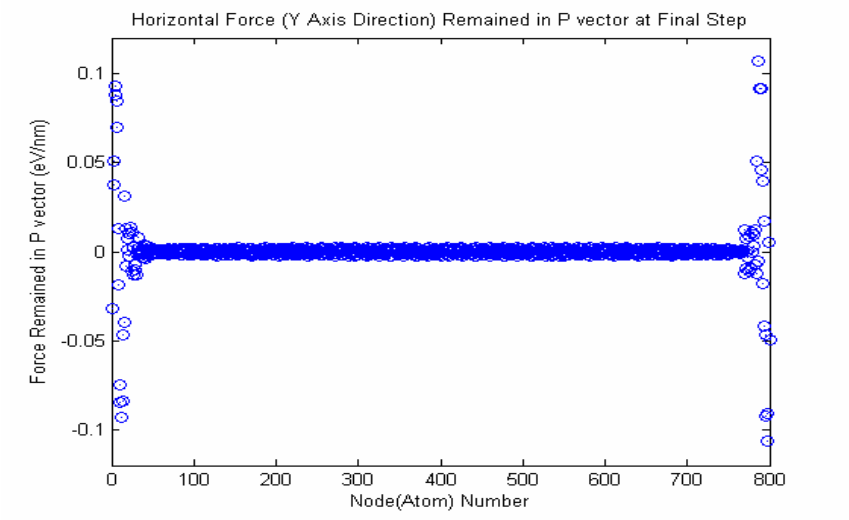

Figure 4.19 - Horizontal Forces Remained in P Vector at Final Stage (Y Direction)

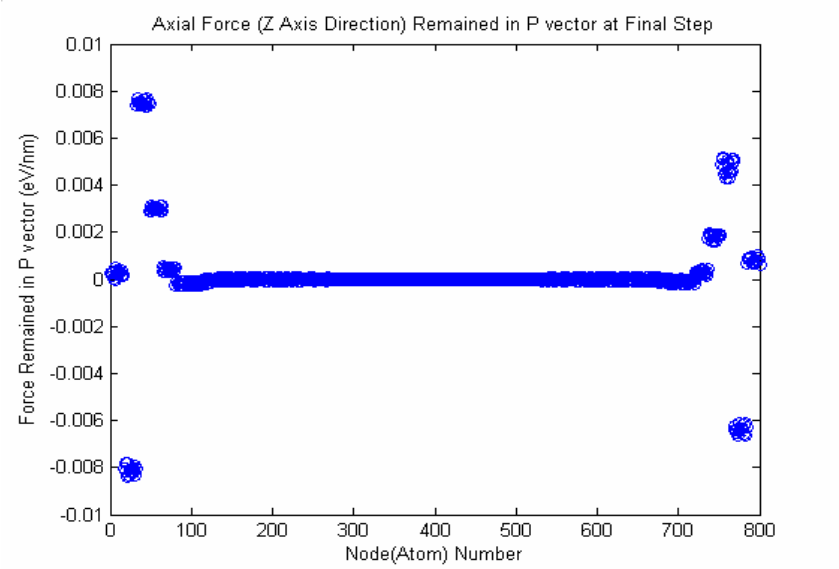

Figure 4.20 - Axial Forces Remained in P Vector at Final Stage (Z Direction)

The horizontal forces in P vector at final stage ranges from 0.1 to -0.1 ev/nm as shown in Figures 4.18 and 4.19. The axial forces in P vector at final stage are much smaller, varying from 0.01 to -0.01 ev/nm. The horizontal movement of atoms is limited due to the horizontal spring boundary condition while the axial movement of atoms is relatively free. Thus, the horizontal components of P vector were minimized more than vertical components. It was impossible to make P vector less than the values shown from Figure 4.18 to 4.20. However, those values in P vector would be small enough, and the nodes away from the boundary have very small forces close to zero.

The compressive external forces were applied on the second layers from the top and bottom as illustrated in Figure 4.15. Calculating the stress requires an area where the external forces are applied. If the hollow carbon nanotube is assumed to be a solid fiber of diameter D, the stress is computed as,

$$\sigma = \frac{Total \quad External \quad Forces \quad at \quad Each \quad Side}{\frac{1}{4} \cdot \pi \cdot D^2} \tag{4.17}$$

where D is the diameter of the CNT. Poisson's ratio of ν is one of the important material properties calculated as,

$$\nu = -\frac{Transverse \quad Contraction \quad Strain}{Longitudinal \quad Strain} = -\frac{\varepsilon_{trans}}{\varepsilon_{longitudinal}} \tag{4.18}$$

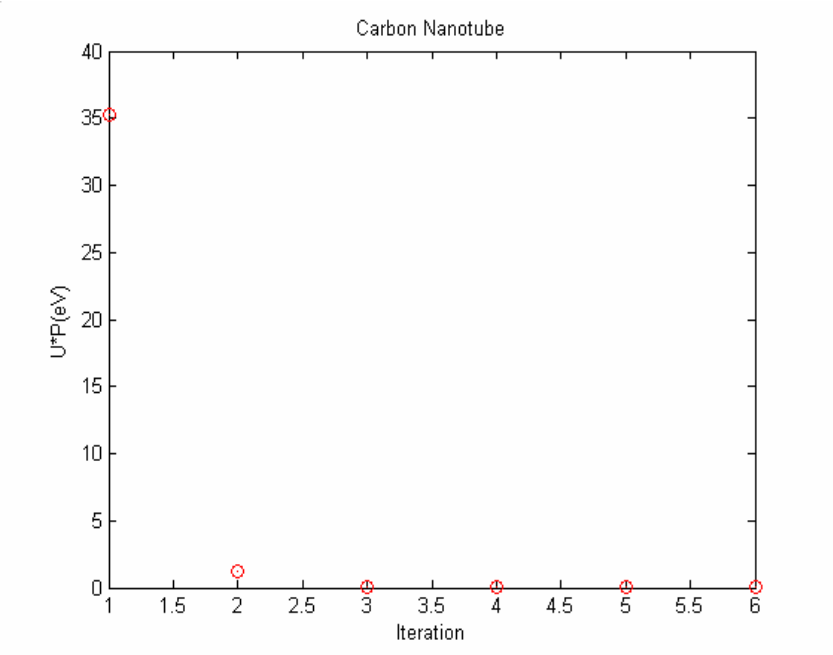

Figure 4.21 - U'·P with Iteration

In 6th iteration, the dot product of U and P becomes less than 10^{-3} eV. Figure 4.21 shows the convergent behavior of CNT using AFEM simulation.

4.4.4 Mechanical Behavior of CNT

Table 4.4 shows the displacements of the CNT against axial compressive forces. Using these data, the stress-strain behavior can be calculated and tabulated in Table 4.5.

Table 4.4 - Deformation of (7,7) Armchir Carbon Nanotube

Compressive Stress (Gpa)	Height (nm)	Diameter (nm)
0	5.8780	1.0599
7.18	5.8247	1.0657
14.21	5.7713	1.0718
21.06	5.7173	1.0780
27.75	5.6626	1.0846
34.24	5.6070	1.0915
37.70	5.5683	1.1010

Table 4.5 - Stress strain Behavior of (7,7) Armchir Carbon Nanotube

Compressive Stress (Gpa)	Vertical Strain (Longitude)	Horizontal Strain (Diameter)	Young's Modulus (Gpa)	Poisson's Ratio
7.18	0.0091	-0.0037	792.6595	0.4033
14.21	0.0182	-0.0074	782.4415	0.4091
21.06	0.0273	-0.0113	770.7392	0.4151
27.75	0.0366	-0.0154	757.3701	0.4215
34.24	0.0461	-0.0198	742.7435	0.4290
37.70	0.0527	-0.0257	715.4813	0.4876
		Average	760.2392	0.4276

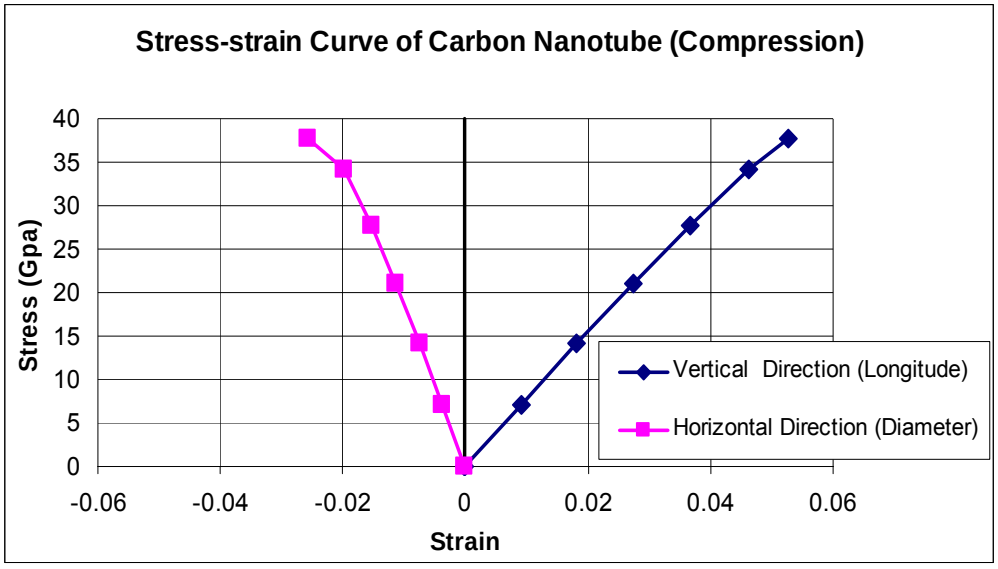

Figure 4.22 - Stress-strain Curve of (7,7) Armchair Carbon Nanotube

As the external forces increase, the longitudinal length becomes smaller, and the diameter becomes greater. Figure 4.22 describes the vertical and horizontal stress-strain relation which is approximately a linear relationship. Young's Modulus of the CNT in average was 760 GPa, and Poisson's ratio was 0.43. At the final stage of loading of 37.7 GPa, the vertical and horizontal displacements are significantly increased, showing instability of the CNT structure.

In fact, if the external stress of 40 GPa is applied on the CNT, the system is unstable, and finally the buckling behavior can be observed as it was described in Figure 4.23. The critical strain is a strain when a material buckles under a certain amount of external forces. The critical strain of CNT reported by Yakobson (1995) is given by,

$$\varepsilon_c = (0.077 \quad nm) \cdot d^{-1} \tag{4.19}$$

where d is the diameter of CNT. Since the diameter is 1.0599 nm, the buckling will take place at a strain of 0.07 which corresponds to the buckling strain of the AFEM simulation in MATLAB.

Interestingly enough, Figure 4.23 can be seen, depending on the direction of observation. Liu et al. (2003), Sears et al. (2006) and Yakobson (1995) also reported similar buckling behaviors of the armchair carbon nanotube.

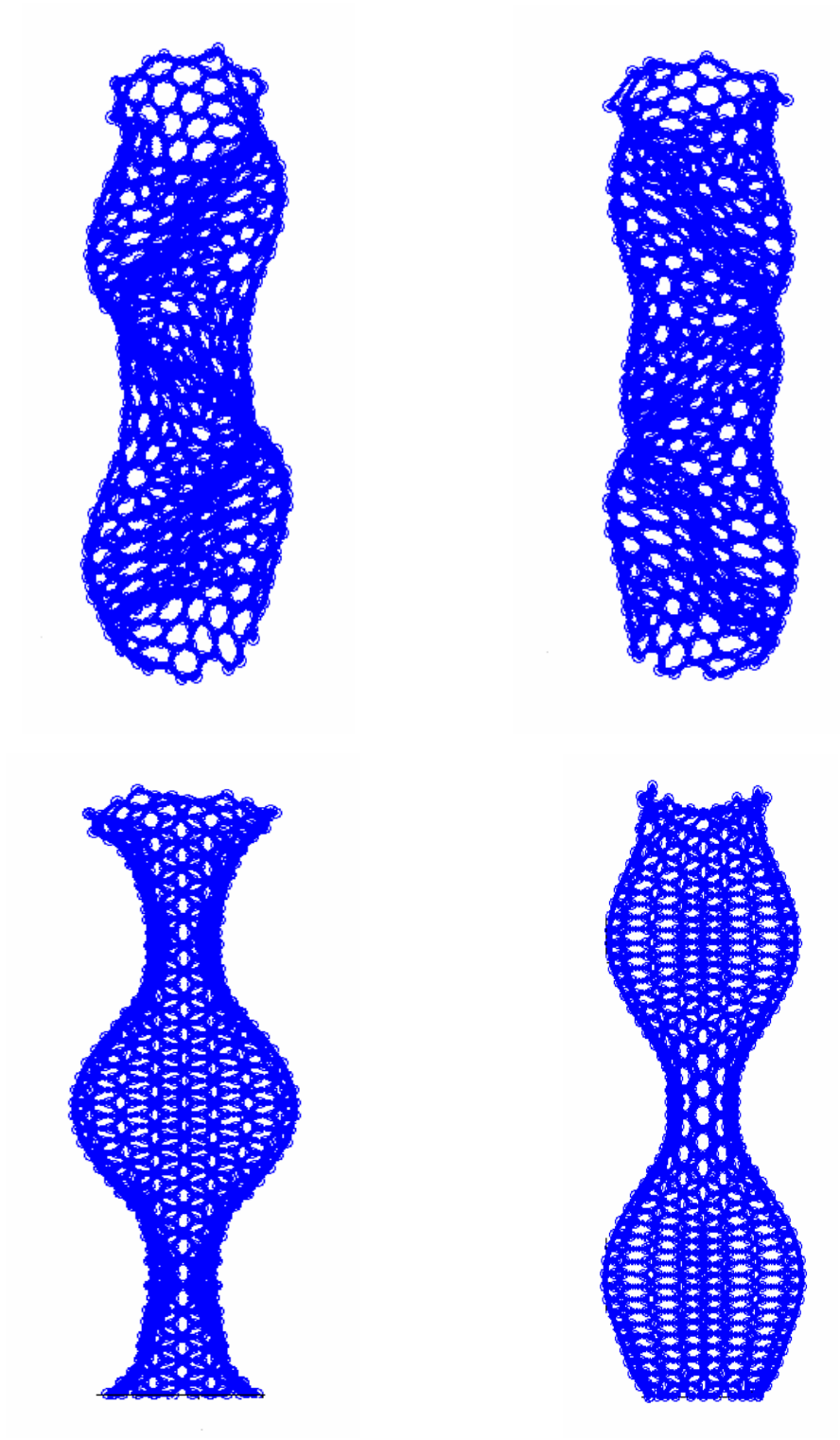

Figure 4.23 - Buckling Behavior of (7, 7) Armchair Carbon Nanotube

4.5 AFEM Application to Quartz

4.5.1 Structure of Quartz

The 892 atoms in quartz were used. The numbers of silicon and oxygen atoms are 380 and 512. The number of tetrahedrons is 380, the same as the number of silicon atoms located at the center of the tetrahedrons. Instead of three-dimensional model, the two-dimensional tetrahedrons were drawn in order to explain the force relationship in quartz.

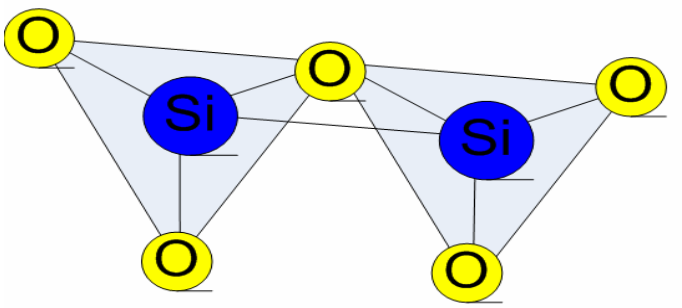

Figure 4.24 - Two Tetrahedrons

The electric forces between silicon and oxygen atoms shown in Figure 4.24 can be interpreted by Figure 4.25.

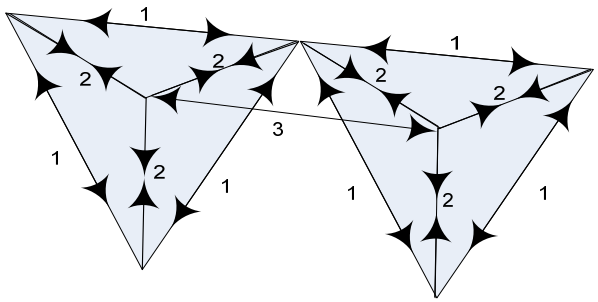

Figure 4.25 - Electric Force Relationship within Tetrahedrons

There is an attractive force between different atoms, and repulsive force between the same atoms. For instance, the attractive force exists in the element number 2 which governs the relationship between silicon and oxygen due to ionic bonding. The oxygen atoms repulse each other, and the same interaction exists between silicon atoms, described in element number 1 and 3 in Figure 4.25, respectively.

4.5.2 Framework of Three-dimensional AFEM Using Pair Potential

Equation 2.9 gives the electric force within the system of quartz. The symmetrical stiffness matrix and nonequilibrium force vector using the pair potential can be written as,

$$\begin{bmatrix} \frac{\partial^2 U_{i-1,i}}{\partial x_{i-1}\partial x_{i-1}} & \frac{\partial^2 U_{i-1,i}}{\partial x_{i-1}\partial y_{i-1}} & \frac{\partial^2 U_{i-1,i}}{\partial x_{i-1}\partial z_{i-1}} & \frac{\partial^2 U_{i-1,i}}{\partial x_{i-1}\partial x_i} & \frac{\partial^2 U_{i-1,i}}{\partial x_{i-1}\partial y_i} & \frac{\partial^2 U_{i-1,i}}{\partial x_{i-1}\partial z_i} \\ \frac{\partial^2 U_{i-1,i}}{\partial y_{i-1}\partial x_{i-1}} & \frac{\partial^2 U_{i-1,i}}{\partial y_{i-1}\partial y_{i-1}} & \frac{\partial^2 U_{i-1,i}}{\partial y_{i-1}\partial z_{i-1}} & \frac{\partial^2 U_{i-1,i}}{\partial y_{i-1}\partial x_i} & \frac{\partial^2 U_{i-1,i}}{\partial y_{i-1}\partial y_i} & \frac{\partial^2 U_{i-1,i}}{\partial y_{i-1}\partial z_i} \\ \frac{\partial^2 U_{i-1,i}}{\partial z_{i-1}\partial x_{i-1}} & \frac{\partial^2 U_{i-1,i}}{\partial z_{i-1}\partial y_{i-1}} & \frac{\partial^2 U_{i-1,i}}{\partial z_{i-1}\partial z_{i-1}} & \frac{\partial^2 U_{i-1,i}}{\partial z_{i-1}\partial x_i} & \frac{\partial^2 U_{i-1,i}}{\partial z_{i-1}\partial y_i} & \frac{\partial^2 U_{i-1,i}}{\partial z_{i-1}\partial z_i} \\ \frac{\partial^2 U_{i-1,i}}{\partial x_i\partial x_{i-1}} & \frac{\partial^2 U_{i-1,i}}{\partial x_i\partial y_{i-1}} & \frac{\partial^2 U_{i-1,i}}{\partial x_i\partial z_{i-1}} & \frac{\partial^2 U_{i-1,i}}{\partial x_i\partial x_i} & \frac{\partial^2 U_{i-1,i}}{\partial x_i\partial y_i} & \frac{\partial^2 U_{i-1,i}}{\partial x_i\partial z_i} \\ \frac{\partial^2 U_{i-1,i}}{\partial y_i\partial x_{i-1}} & \frac{\partial^2 U_{i-1,i}}{\partial y_i\partial y_{i-1}} & \frac{\partial^2 U_{i-1,i}}{\partial y_i\partial z_{i-1}} & \frac{\partial^2 U_{i-1,i}}{\partial y_i\partial x_i} & \frac{\partial^2 U_{i-1,i}}{\partial y_i\partial y_i} & \frac{\partial^2 U_{i-1,i}}{\partial y_i\partial z_i} \\ \frac{\partial^2 U_{i-1,i}}{\partial z_i\partial x_{i-1}} & \frac{\partial^2 U_{i-1,i}}{\partial z_i\partial y_{i-1}} & \frac{\partial^2 U_{i-1,i}}{\partial z_i\partial z_{i-1}} & \frac{\partial^2 U_{i-1,i}}{\partial z_i\partial x_i} & \frac{\partial^2 U_{i-1,i}}{\partial z_i\partial y_i} & \frac{\partial^2 U_{i-1,i}}{\partial z_i\partial z_i} \end{bmatrix} \begin{bmatrix} u_{x,(i-1)} \\ u_{y,(i-1)} \\ u_{z,(i-1)} \\ u_{x,(i)} \\ u_{y,(i)} \\ u_{z,(i)} \end{bmatrix} = \begin{bmatrix} -\frac{\partial U_{i-1,i}}{\partial x_{i-1}} \\ -\frac{\partial U_{i-1,i}}{\partial y_{i-1}} \\ -\frac{\partial U_{i-1,i}}{\partial z_{i-1}} \\ -\frac{\partial U_{i-1,i}}{\partial x_i} \\ -\frac{\partial U_{i-1,i}}{\partial y_i} \\ -\frac{\partial U_{i-1,i}}{\partial z_i} \end{bmatrix} \quad (4.20)$$

As was discussed in Equation 4.5 and 4.8, the external forces can be added on the corresponding addresses in the nonequilibrium force vector.

4.5.3 Limitation of Potential Energy for Quartz

The electrostatic forces have an influence on all atoms in the system. Moreover, it affects on the imaginary atoms in the system introduced by the periodic boundary condition. In the screened Coulomb term of Equation 2.7, the cutoff distance of 0.55 nm should be employed. However, in this research, the periodic boundary was difficult to be constructed. Instead, the periodic boundary condition was ignored in order to simplify the modeling. It was supposed that the forces act between the nearest neighbor atoms such as silicon and oxygen, oxygen and oxygen and silicon and silicon atoms, shown in Figure 4.24. The maximum length was 0.31 nm between silicon and silicon atoms on average.

4.5.4 Boundary Condition and External forces

The silicon atoms at the bottom of the quartz were fixed. The external force was applied at the top of the quartz. It should be noted that the boundary condition and external force of quartz were applied on the silicon atoms at the center of tetrahedrons. Figure 4.26 shows the area of external force applied and x, y and z axis in Cartesian coordinate. The quartz has a trigonal symmetry with $\alpha=\beta=90°$ and $\gamma=120°$. During simulation, it was observed that several tetrahedrons were obtruded at the surface of the quartz as can be seen in Figure 4.26. It is owing to the ionic repulsion between silicon and silicon atoms. The role of the periodic boundary condition which was not developed here would be to confine the obtruded tetrahedrons.

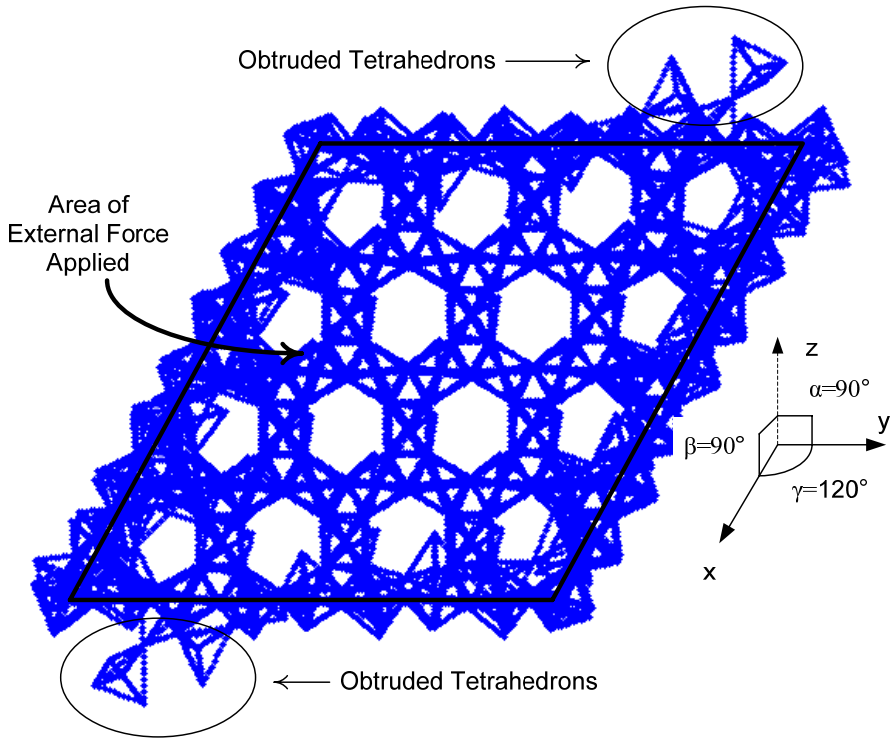

Figure 4.26 - Plan View of Quartz (892 Atoms)

4.5.5 Mechanical Behavior of Quartz

Table 4.6 - Stress Strain Behavior of Quartz

External Stress (Gpa)	0.726	1.443	2.14	3.47	4.74	5.91	6.6	7.78
ε_{XX}	-0.0027	-0.0054	-0.0084	-0.0150	-0.0225	-0.0305	-0.0345	-0.0460
ε_{yy}	-0.0033	-0.0068	-0.0108	-0.0200	-0.0290	-0.0375	-0.0425	-0.0500
ε_{zz}	0.0058	0.0116	0.0175	0.0300	0.0430	0.0560	0.0620	0.0715
ε_{YZ}	-0.0145	-0.0265	-0.0420	-0.0770	-0.1150	-0.1560	-0.1800	-0.2300
ε_{ZX}	0.0001	0.0001	0.0000	-0.0010	-0.0032	-0.0072	-0.0104	-0.0240
ε_{XY}	0.0058	0.0100	0.0108	0.0139	0.0215	0.0440	0.0575	0.0820

The axial force is applied on quartz in z axis in Figure 4.26. Thus, Young's modulus of quartz against vertically applied forces in z direction is 115 Gpa and, Poisson's ratios are

0.52 in x direction and 0.65 in y direction, obtained from Table 4.4 and Figure 4.26. Although Young's modulus of quartz is reasonable, the Poisson's ratios are too high over the highest Poisson's ratio of 0.5. In addition, the shear strain of yz direction is too high.

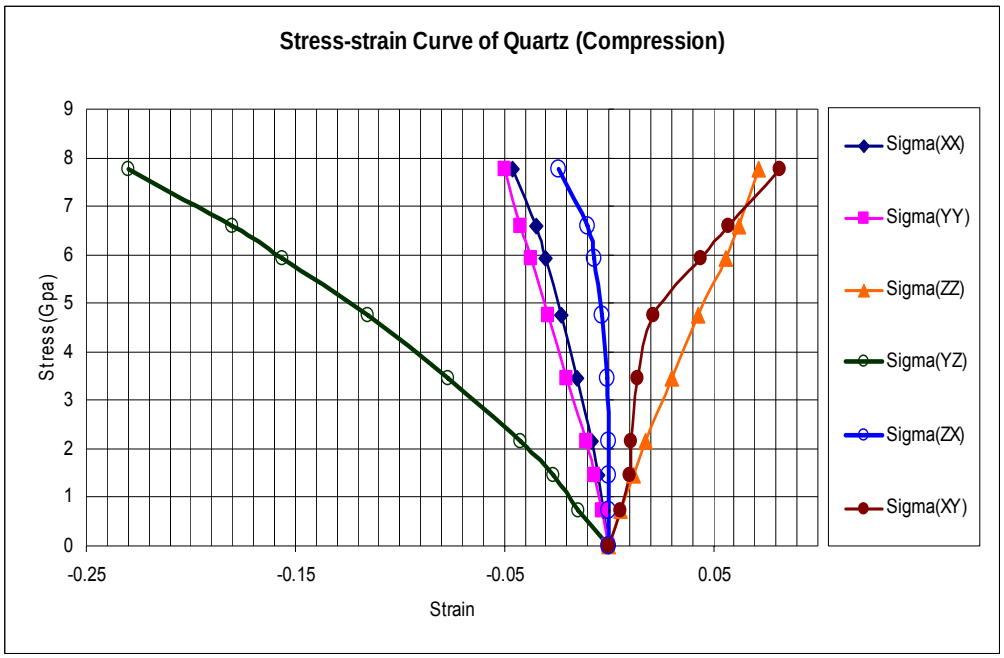

Figure 4.27 - Stress Strain Curve of Quartz

It might be due to the assumption about the periodic boundary condition and the cutoff distance of 0.55 nm neglected in this AFEM simulation. This result potentially shows the importance of periodic boundary condition and cutoff distance. Garofalini (1981) and Kuzuu at al. (2004) also point out the significance of the cutoff distance.

This AFEM application to quartz does not provide an accurate result, compared with MD simulation previously conducted. However, it is meaningful that the modified Born-Mayer-Huggins potential connecting the nearest atoms works in AFEM simulation.

The potential problem of AFEM when applied to analyze minerals is the electrostatic force which considers too many atoms around one atom. Then, the stiffness matrix is not sparse

any more. Thus, inverting K matrix takes a long time. It is also expected that the optimization may not work very well if too many electrostatic force conditions need to be satisfied.

Chapter 5 Conclusion and Recommendation for Future Research

5.1 Conclusion

The purpose of this research was to introduce the mechanism of AFEM based on the energy minimizing principle. After atoms are moved by internal and external forces, the nonequilibrium force vector finally approaches zero, satisfying Newton's third law. The validation of AFEM was conducted by comparing displacement of a simple model with MD in one dimensional space. The frameworks of AFEM using pair potentials work well from 1 to 3 dimensions in atomic systems. The speed of AFEM was checked with MATLAB software using the vectorization scheme and sparse command. Although the speed of one-dimensional AFEM was slightly nonlinear with respect to the number of atoms, two-dimensional AFEM results in a linear relationship between the computational time and the number of atoms under the systems of 2000 atoms or less.

The traditional boundary condition is difficult to apply in AFEM. Instead, the spring boundary condition was proposed for analyzing the mechanical behavior of the CNT. In another case, after the bottom of the CNT was clamped and the CNT was uniaxially compressed, the buckling behavior was observed, similar to the results of the previous MD research. The mechanical behavior of Quartz was analyzed with the modified Born-Mayer-Huggins potential. Since the periodic boundary condition and cutoff of 0.55 nm was ignored, the high Poisson's ratio was obtained. The conclusions of this research can be summarized as follows.

1. AFEM and MD have a similar theoretical framework, but MD does not make all nodal forces zero simultaneously while atoms in AFEM should be in equilibrium at the same time.

2. The computational time of AFEM is approximately proportional to the number of atoms, and the absolute computational time is small enough with the vectorization scheme and sparse command.
3. The spring boundary condition for the CNT works.
4. Young's Modulus and Poisson's ratio of single wall (7,7) armchair carbon nanotube are 760 GPa and 0.43, respectively when it is regarded as a solid fiber of diameter equal to that of the carbon nanotube.
5. Young's Modulus of quartz is 115 GPa but Poisson's ratio of 0.5 of quartz is not realistic since the periodic boundary condition and cutoff distance were ignored. The nonequilibrium vector becomes zero if the nearest neighboring atoms are connected for silicon and silicon atoms, oxygen and oxygen atoms and silicon and oxygen atoms.
6. The stiffness matrix of AFEM may not be sparse anymore when the electrostatic force is employed, possibly resulting in reduced efficiency of AFEM.

5.2 Recommendation for Future Research

The electrostatic force and periodic boundary condition could not be applied for AFEM simulation of quartz and should be studied in later research of AFEM. Another future research is to study AFEM coupled with the continuum finite element method. In an atomic system, AFEM can be used where the large deformation is expected or its displacement is important. Otherwise, the continuum finite element method can replace AFEM in order to reduce the number of degrees of freedom. Therefore, the combination of AFEM and the continuum finite element method provide the multi-scale computation method, making it possible to augment the size of the system to be simulated.

References

Brenner, Donald W. (1991). Empirical Potential for Hydrocarbons for Used in Simulating the Chemical Vapor Deposition of Diamond Films. Physical Review B. Vol. 42(15), pp. 9458-9470

Feuston, B.P., Garofalini, S. H. (1988). Empirical Three-body Potential for Vitreous Silica. Chemical Physics. Vol. 89 (9), pp. 5818-5824

Fosdick Lloyd D. (1995). Molecular dynamics: An Introduction. HPSC Course Notes High Performance Scientific Computing University of Colorado at Boulder. Pp. 1-49

Garofalini, Stephen H. (1981). Molecular Dynamics Simulation of the Frequency Spectrum of Amorphous Silica. Chemical Physics. Vol. 76, pp. 3189-3192

Gates, T.S., Odegard, G.M., Frankland, S.J.V., Clancy, T.C. (2005). Computational Materials: Multi-scale Modeling and Simulation of Nanostructured Materials. Composites Science and Technology. Vol. 65, pp. 2416-2434

Griebel Michael, Hamaekers Jan. (2003). Molecular Dynamics Simulations of the Elastic Moduli of Polymer-carbon Nanotube Composites. Computer Methods in Applied Mechanics and Engineering. Vol. 193 pp. 1773-1778

Hochella, Michale F. (2001). There's Planty of Room at the Bottom. Geochimica et Cosmochimica Acta. Vol. 66(5), pp. 735-743

Ichikawa, Yasuaki, Kawamura, Katsuyuki, Theramast, Nattavut, Kitayama, Kazumi. (2004). Secondary and Tertial Consolidation of Bentonite Clay: Consolidation Test, Molecular Dyanmics Simulation and Multiscale Homogenization Analysis. Mechanics of Materials. Vol. 36. pp. 487-513

Kuzuu, Nobu, Yoshie, Hiroki, Tamai, Yoshinori, Wang, Chen. (2004). Molecular Dyanmics Study of Temperature Dependence of Volume of Amorphous Silica. Journal of Non-crystalline Solids. Vol. 349, pp. 319-330

Leach, Andrew R. (2001). Molecular Modelling: Principles and Applications. Prentice Hall.

Liu, B., Huang, Y., Jiang, H., Qu, S., Hwang, K.C. (2004). The Atomic Scale Finite Element Method. Computer Methods in Applied Mechanics and Engineering. Vol. 193, pp. 1849-1864

Liu, B., Jiang, H., Johnson, H.T., Huang, Y. (2003). The Influence of Mechanical Deformation on the Electrical Properties of Single Wall Carbon Nanotubes. Journal of the Mechanics and Physics of Solids. Vol. 52, pp. 1-26

Liu, B., Huang, Y., Jiang, H., Qu, S., Hwang, K.C. (2004). The Atomic-scale Finite Element Method. Computer Methods in Applied Mechanics and Engineering. Vol. 193, pp 1849-1864

Liu, B., Huang, Y., Jiang, H., Qu, S., Hwang, K.C. (2004). Finite Element Method: From Discrete Atoms to Continuum Solids, Handbook of Theoretical and Computational Nanotechnology (Chapter 100) , Vol. 1, pp. 1-19

Logan Daryl L. (1992). A First Course in the Finite Element Method. PWS Publishing Company. pp. 37-47

Mitchell, James K., Santamarina, Carlos (2005) Biological Considerations in Geotechnical Engineering. Journal of Geotechnical and Geoenvironmental Engineering. Vol. 131(10), pp. 1222-1232

Mamalis A.G. Vogtlander L.O.G. Markopoulos A. (2002). Nanotechnology and Nanostructured Materials: Trends in Carbon Nanotubes. Precision Engineering. Vol. 28, pp. 16-30

Robinett Richard W. (1997) Quantum Mechanics. Oxford University Press.

Sears A. and Batra Romesh C. (2006). Buckling of Multiwalled Carbon Nanotubes under Axial Compression. Physical Review B 73(085410), pp. 1-11

Seminario Jorge M. (1996). Calculation of Intramolecular Force Fields from Second–Derivative Tensors. International Journal of Quantum Chemistry: Quantum Chemistry Symposium Vol. 30, pp. 59-65

Tersoff J. (1987). New Empirical Approach for the Structure and Energy of Covalent Systems. Physical Review. Vol. 37(12), pp. 6991-7000

Yakobson, B.I., Brabec, C.J., Bernholc., J. (1995). Nanomechanics of Carbon Tubes: Instabilities beyond Linear Response. Physical Review Letters Vol. 76(14), pp. 2511-2514

Zhang, P., Huang, Y., Geubelle, P.H., Klein, P.A., Hwang, K.C. (2002). The Elastic Modulus of Single-wall Carbon Nanotubes: A Continuum Analysis Incorporating Interatomic Potentials. International Journal of Solid and Structures. Vol. 39, pp. 3893-3906

Vita

Kyusang Kim

I was born in March 7, 1978 and raised in Jeollabukdo, South Korea. After graduating from Namsung High School, I attended Konkuk University in Seoul, South Korea and graduated in February 2003, receiving Bachelor of Science in Civil Engineering. Then I studied the geotechnical engineering in Civil Engineering at Virginia Polytechnic Institute and State University and achieved Master of Science degree in August 2006. I am interested in the numerical modeling and geophysical methods.